DRAFT
CMS Paper

The content of this note is intended for CMS internal use and distribution only

An inclusive search for new phenomena in final states with one or more jets and missing transverse momentum at $\sqrt{s} = 13\,\text{TeV}$ with the α_T variable

The CMS Collaboration

Abstract

An inclusive search for new-physics phenomena is performed in final states containing one or more jets and an imbalance in transverse momentum in pp collisions at a centre-of-mass energy of 13 TeV. The analysed data sample, recorded with the CMS detector at the CERN Large Hadron Collider, corresponds to an integrated luminosity of $2.3\,\text{fb}^{-1}$. Several kinematical variables are employed to strongly suppress the dominant background, multijet production from quantum chromodynamics, as well as discriminate effectively between other standard model and new-physics processes. The search provides sensitivity to a broad range of the new-physics models that yield a stable weakly interacting massive particle. The observed candidate events are found to agree with the expected contributions from standard model processes, and the result is interpreted in the mass parameter space of fifteen simplified supersymmetric models that assume the pair production of gluinos or squarks, and a range of decay modes.

Contents

1   Introduction

The standard model (SM) of particle physics is successful in describing a wide range of phenomena, and the model is currently being extensively tested at high energies with collider-based experiments. To date, no contrary evidence has yet been attained. Nevertheless, the SM is widely believed to be only an effective approximation of a more complete theory that supersedes it at a higher energy scale. Supersymmetry (SUSY) [1–8] is a complete, renormalisable extension to the Standard Model (SM) that exploits the unique way to extend the space-time symmetry group underpinning the SM. For each boson (fermion) in the SM, a fermionic (bosonic) superpartner, which differs in spin by one-half unit, is introduced.

The proposed supersymmetric extension to the SM is compelling from theoretical, phenomenological, and experimental considerations. From a theory perspective, the addition of super-partners to SM particles can modify the running of the gauge coupling constants such that their unification can be achieved at a high scale. Experimentally, SUSY is a testable extension through the postulate of an extensive array of new observable states (of unknown masses). The gluinos $\widetilde{g}$, light- and heavy-flavour squarks $\widetilde{q}, \widetilde{b}, \widetilde{t}$, and sleptons $\widetilde{\ell}$ are, respectively, the super-partners to gluons, quarks, and leptons. An extended Higgs sector is also postulated, as well as four neutralino $\widetilde{\chi}_{1,2,3,4}^0$ and two chargino $\widetilde{\chi}_{1,2}^{\pm}$ states that arise from the mixing between the superpartner states to neutral and charged Higgs bosons and the electroweak gauge bosons.

A more topical perspective, given the recently discovered Higgs boson [9, 10], is the conjecture that the superpartners ("sparticles") can alleviate the gauge hierarchy problem of the SM, by compensating for radiative corrections to the Higgs mass from loop processes involving SM particles. These corrections diverge according to a power-law dependence on scale, which can only be accommodated in the SM through an extreme level of fine tuning of the bare Higgs

44 mass parameter. A "natural" solution, with minimal fine-tuning, requires the $\widetilde{t}_L$, $\widetilde{t}_R$, $\widetilde{b}_L$, and
45 $\widetilde{g}$ to be realised at or near the electroweak scale. These "natural" constraints, which can be
46 relaxed at the expense of the level of fine tuning, imply the presence of states accessible by the
47 CERN Large Hadron Collider (LHC).

48 Finally, the assumption of R-parity conservation [11] has important consequences for cosmol-
49 ogy and collider phenomenology. SUSY particles are expected to be produced in pairs at the
50 LHC, with heavy states decaying to the lightest stable supersymmetric particle (LSP). The LSP
51 is generally assumed to be the $\widetilde{\chi}_1^0$, which is weakly interacting and massive. This sparticle is
52 considered to be a Dark Matter (DM) candidate, the existence of which is supported by astro-
53 physical data []. Hence, the characteristic signature of "natural" SUSY production at the LHC
54 is a final state containing an abundance of jets, possibly originating from top or bottom quarks,
55 accompanied by a significant transverse momentum imbalance, $\vec{p}_T^{\text{miss}}$.

56 The lack of evidence to date for SUSY has also focused the attention on regions of the parameter
57 space with weak coverage. For example, models in which both the $\widetilde{t}$ and the $\widetilde{\chi}_1^0$ are light and
58 nearly degenerate in mass are phenomenologically well motivated []. This class of models, with
59 "compressed" mass spectra, typically yields SM particles with very low momenta from the
60 decays of sparticles. Hence, searches rely on the associated production of jets, often resulting
61 from initial-state radiation (ISR), to achieve nonnegligible experimental acceptance.

62 This article presents an inclusive search for new-physics phenomena in hadronic final states
63 with one or more energetic jets and an imbalance in transverse momentum, performed in pp
64 collisions at a centre-of-mass energy $\sqrt{s} = 13\,\text{TeV}$. The analysed data sample corresponds to
65 an integrated luminosity of $2.3 \pm 0.1\,\text{fb}^{-1}$ [?] collected by the Compact Muon Solenoid (CMS)
66 experiment. Previous iterations of this search have been performed in pp collisions at both
67 $\sqrt{s} = 7$ [12–14] and 8 TeV [15 ?].

68 The increase in the centre-of-mass energy of the LHC, from $\sqrt{s} = 8$ to 13 TeV, provides a unique
69 opportunity to search for the characteristic signatures of new physics at the TeV scale. For
70 example, the increase in $\sqrt{s}$ leads to a factor $\gtrsim 35$ increase in the parton luminosity for the pair
71 production of coloured supersymmetric particles, each of mass 1.5 TeV, which were beyond
72 the reach of searches performed at $\sqrt{s} = 8\,\text{TeV}$. Several searches have already provided results
73 with the first data, interpreted within the context of SUSY, at this new energy frontier [].

74 In this search, to ensure sensitivity to the broadest possible region of the supersymmetric pa-
75 rameter space, an inclusive strategy is adopted, which focuses on maintaining high acceptance,
76 through the application of selection criteria with the lowest possible thresholds, and the cate-
77 gorisation of candidate signal events according to multiple discriminating variables.

78 It is noted here that the search is sufficiently generic and inclusive to provide sensitivity to a
79 wide range of nonsupersymmetric models that postulate the existence of a stable, weakly inter-
80 acting, massive particle, assumed to be consistent with the nature of DM. In addition to the jets
81 + $\vec{p}_T^{\text{miss}}$ topology, the search now considers final states containing a "monojet" + $\vec{p}_T^{\text{miss}}$ topology,
82 which is expected to improve the sensitivity to DM particle production in pp collisions [16, 17].

83 This search is based on an examination of the number of reconstructed jets per event, the num-
84 ber of these jets identified as originating from bottom quarks, and the scalar and vector sums of
85 transverse momenta of these jets. These variables provide sensitivity to the different produc-
86 tion mechanisms of massive coloured sparticles at hadron colliders (i.e. squark-squark, squark-
87 gluino, and gluino-gluino), "natural" third-generation squark signatures, and both large and
88 small mass splittings between the parent sparticle and the LSP.

The dominant background process for a search in all-jet final states is multijet production, a manifestation of quantum chromodynamics (QCD). An accurate estimate of this background contribution is difficult to achieve, given the lack of precise theoretical predictions for the multijet production cross section and kinematical properties.

The search is built around the kinematical variable α_{T} [12, 18], which provides powerful discrimination against multijet production. The α_{T} variable is constructed from jet-based quantities and provides discrimination between "genuine" sources of transverse momentum imbalance, from stable, weakly interacting particles, such as neutrinos or neutralinos, that escape the detector, and "fake" sources, such as the mismeasurement of jet energies. The $\Delta\phi^*_{\min}$ [12] variable exploits azimuthal angular information and also provides strong rejection power against multijet events, including rare energetic events in which neutrinos carry a significant fraction of the energy of a jet, due to semileptonic decays of heavy-flavour mesons. These two variables are designed to provide robust discrimination against multijet events at the energy and luminosity frontier, and very restrictive requirements on the α_{T} and $\Delta\phi^*_{\min}$ variables are employed in this search.

The organization of this article is as follows. Sections 2 and 3 describe, respectively, the CMS apparatus and the simulated event samples. Sections 4 and 5 describe the event reconstruction and selection criteria used to identify candidate signal events and control region samples. Section 6 provides details on the estimation of the multijet and all other SM backgrounds. Finally, the search results and interpretations, in terms of simplified supersymmetric models, are described in Sections 7 and 8, and summarised in Section 9.

2 The CMS detector

The central feature of the CMS apparatus is a superconducting solenoid of 6 m internal diameter, providing an axial magnetic field of 3.8 T. The bore of the solenoid is instrumented with several particle detection systems. A silicon pixel and strip tracker measures charged particles within the pseudorapidity [19] range $|\eta| < 2.5$. A lead tungstate crystal electromagnetic calorimeter (ECAL), and a brass and scintillator hadron calorimeter (HCAL), each composed of a barrel and two endcap sections, extend over a pseudorapidity range $|\eta| < 3.0$. Outside the bore of the solenoid, forward calorimeters extend the pseudorapidity coverage to $|\eta| < 5.0$, and muons are measured within $|\eta| < 2.4$ by gas-ionization detectors embedded in the steel flux-return yoke outside the solenoid. A two-tier trigger system selects pp collision events of interest. The first level (L1) of the trigger system, composed of custom hardware processors, uses information from the calorimeters and muon detectors to select the most interesting events in a fixed time interval of less than $4\,\mu$s. The high-level trigger (HLT) processor farm further decreases the event rate from around 100 kHz to less than 1 kHz, before data storage. The CMS detector is nearly hermetic, which allows for momentum-balance measurements in the plane transverse to the beam axis. A more detailed description of the CMS detector, together with a definition of the coordinate system used and the relevant kinematic variables, can be found in Ref. [19].

3 Simulated event samples

The search relies on multiple event samples, in data or generated from Monte Carlo (MC) simulations, to estimate the contributions from SM backgrounds, as described in Section 5. The dominant SM backgrounds for the search are QCD multijet production, and the associated production of jets and top-antitop ($t\bar{t}$), single top, and vector boson (W, $Z \to \nu\bar{\nu}$). Residual

133 contributions from other processes, such as WW, WZ, ZZ (diboson) production and the associ-
134 ated production of t$\bar{\text{t}}$ and a vector boson (W and Z), are also considered. Other processes, such
135 as Drell-Yan (q$\bar{\text{q}} \to$ Z/$\gamma^* \to \ell^+\ell^-$) and γ+jets production, are also relevant for some control
136 regions, defined in Section 5.5.

137 The MADGRAPH 5 aMC@NLO 2.2.2 [20] event generator code is used at leading order (LO)
138 accuracy to produce samples of W+jets, Z+jets, γ+jets, t$\bar{\text{t}}$, and multijet events. The same code
139 is used at next-to-leading order (NLO) accuracy to generate samples of single top (both s- and
140 t-channel production), WZ, ZZ, t$\bar{\text{t}}$W, and t$\bar{\text{t}}$Z events. The NLO POWHEG v2 [21, 22] generator is
141 used to describe WW events and the Wt-channel production of single top events. The simulated
142 samples are normalised according to production cross sections that are calculated with NLO
143 and next-to-NLO precision [20, 22–27]. The description of the detector response is implemented
144 using the GEANT4 [28] package.

145 Event samples for signal models involving gluino or squark pair production, in association
146 with up to two additional partons, are generated at leading order with MADGRAPH 5 aMC@NLO,
147 and the decay of the sparticles is performed with PYTHIA 8.2 [29]. Inclusive, process-dependent,
148 signal production cross sections are calculated with NLO plus next-to-leading-logarithm (NLL)
149 accuracy [30–35]. The detector response is provided by the CMS fast simulation package [36].

150 The NNPDF3.0 LO and NNPDF3.0 NLO [37] parton distribution functions (PDF) are used,
151 respectively, with the LO and NLO generators described above. The LO PYTHIA 8.2 [29] pro-
152 gram is used to describe parton showering and hadronisation for all simulated samples. To
153 model the effects of multiple pp collisions within the same or neighboring bunch crossings
154 (pileup), all simulated events are generated with a nominal distribution of pp interactions per
155 bunch crossing and then reweighted to match the pileup distribution as measured in data. Fi-
156 nally, (near-unity) corrections to the normalisation of the simulated samples for the γ+jets,
157 W($\to \mu\nu$)+jets, t$\bar{\text{t}}$, and Z($\to \mu\mu$)+jets, and, equivalently, Z($\to \nu\bar{\nu}$)+jets processes are derived
158 using a data sideband to the control regions.

4   Event reconstruction

160 Global event reconstruction is provided by the particle-flow (PF) algorithm [38, 39], which aims
161 to identify each single particle using an optimized combination of information from all detector
162 systems. In this process, the identification of the particle type (photon, electron, muon, charged
163 hadron, neutral hadron) plays an important rôle in the determination of the particle direction
164 and energy.

165 The primary vertex (PV) for each recorded event is assumed to be the reconstructed vertex
166 with the largest sum of charged-track p_{T}^2 values that is found within 24 cm and 2 cm of the
167 center of the detector in the direction, respectively, along and perpendicular to the beam axis.
168 Charged tracks associated to reconstructed vertices coincident with the beam axis from other
169 pp interactions within the same or neighbouring bunch crossings (pileup) are not considered
170 by the PF algorithm as part of the global event reconstruction.

171 Photons [40] are identified as ECAL energy clusters not linked to the extrapolation of any
172 charged particle trajectory to the ECAL. The energy of photons is directly obtained from the
173 ECAL measurement, corrected for zero-suppression and pileup effects. Electrons [41] are iden-
174 tified as a charged particle track associated with an ECAL cluster compatible with the track tra-
175 jectory, as well as many additional ECAL energy clusters from potential bremsstrahlung pho-
176 tons emitted as the electron traverses material of the silicon tracker. The energy of electrons is

determined from a combination of the track momentum at the main interaction vertex, the corresponding ECAL cluster energy, and the energy sum of all bremsstrahlung photons attached to the track. Muons [42] are identified as a track in the silicon tracker consistent with either a track or several hits in the muon system and associated with an energy deficit in the calorimeters. The energy of muons is obtained from the corresponding track momentum. Charged hadrons are identified as charged particle tracks neither identified as electrons, nor as muons. The energy of charged hadrons is determined from a combination of the track momentum and the corresponding ECAL and HCAL energy, corrected for zero-suppression effects and for the response function of the calorimeters to hadronic showers. Neutral hadrons are identified as HCAL energy clusters not linked to any charged hadron trajectory, or as ECAL and HCAL energy excesses with respect to the expected charged hadron energy deposit. The energy of neutral hadrons is obtained from the corresponding corrected ECAL and HCAL energy.

Various quality-related criteria must be satisfied in order to identify photons with high efficiency while minimising the misidentification of electrons and associated bremstrahlung, jets, or ECAL noise as photons. The criteria include the following: the shower shape of the energy deposition in the ECAL must be consistent with that expected from a photon, the energy detected in the HCAL behind the photon shower must not exceed 5% of the photon energy, and no matched hits in the pixel tracker must be found. Similar criteria related to the ECAL shower shape and the relative contributions to the total energy deposited in the ECAL and HCAL must be satisfied to identify electrons, with additional requirements on the associated track that consider the track quality, energy-momentum matching, and compatibility with the PV in terms of the transverse and longitudinal impact parameters.

Photons are required to be isolated from other activity in the event, such as charged and neutral hadrons, within a cone $\Delta R = \sqrt{(\Delta\phi)^2 + (\Delta\eta)^2} = 0.3$ around the photon trajectory, corrected for pileup effects and for contributions from the photon itself. Electrons and muons are also required to be isolated from other activity in the event, primarily to suppress background contributions from semileptonic heavy flavour decays in multijet events. The isolation $I_{\rm rel}^{\rm mini}$ is defined as the scalar $p_{\rm T}$ sum of all charged and neutral hadrons and photons within a cone around the lepton direction, divided by the lepton $p_{\rm T}$. The cone radius is dependent on the lepton $p_{\rm T}$, primarily to identify with high efficiency the collimated daughter particles of leptonically decaying Lorentz-boosted top quarks, according to the following: $R = 0.2$ and 0.05 for, respectively, $p_{\rm T} < 50\,{\rm GeV}$ and $p_{\rm T} > 200\,{\rm GeV}$, and $R = 10\,{\rm GeV}/p_{\rm T}$ for $50 < p_{\rm T} < 200\,{\rm GeV}$. The variable $I_{\rm rel}^{\rm mini}$ excludes contributions from the lepton itself and is corrected for the effects of pileup. The isolation for electrons and muons is required to satisfy, respectively, $I_{\rm rel}^{\rm mini} < 0.1$ and 0.2 when considering events with nonleptonic final states. A tighter definition of muon isolation, $I_{\rm rel}^{\mu}$, is used when events are required to contain at least one muon. The variable $I_{\rm rel}^{\mu}$ is determined identically to $I_{\rm rel}^{\rm mini}$ except that a cone of fixed radius $R = 0.4$ is assumed.

Electron and muon candidates identified by the PF algorithm that do not satisfy the quality criteria or the $I_{\rm rel}^{\rm mini}$ isolation requirements described above, as well as charged hadrons, are collectively labeled as "single isolated tracks" if they are isolated from neighbouring charged tracks associated to the PV. The isolation $I_{\rm rel}^{\rm track}$ is defined as the scalar $p_{\rm T}$ sum of charged tracks (excluding the track under consideration) within a cone $\Delta R < 0.3$ around the track direction, divided by the track $p_{\rm T}$. The requirement $I_{\rm rel}^{\rm track} < 0.1$ is imposed.

Jets are clustered from the PF candidate particles with the infrared and collinear safe anti-k_t algorithm [43], operated with a radius parameter R of 0.4. The jet momentum is determined as the vectorial sum of all particle momenta in this jet, and is found in the simulation to be within 5 to 10% of the true momentum over the whole $p_{\rm T}$ spectrum and detector acceptance. Jet energy

corrections, to account for pileup [44] and to establish a uniform relative response in η and a calibrated absolute response in p_{T}, are derived from the simulation, and are confirmed with in situ measurements with the energy balance of dijet and photon+jet events [45]. The jet energy resolution amounts typically to 15% at 10 GeV, 8% at 100 GeV, and 4% at 1 TeV, to be compared to about 40%, 12%, and 5% obtained when the calorimeters alone are used for jet clustering. All jets are required to satisfy loose requirements on the relative composition of their particle constituents to reject noise in the calorimeter systems or failures in event reconstruction.

Jets are identified as originating from b quarks using the combined secondary vertex algorithm [46]. Control regions in data [47] are used to measure the probability to correctly identify jets as originating from b quarks (the b-tagging efficiency), the probability to misidentify jets originating from light-flavour partons (u, d, s quarks or gluons) or a charm quark as a b-tagged jet (the light-flavour and charm mistag probabilities). A working point is employed that yields a b-tagging efficiency, and light-flavour and charm mistag probabilities of, respectively, approximately 65%, 12%, and 1% for jets with transverse momenta typical of $t\bar{t}$ events.

The missing transverse momentum vector $\vec{p}_{\mathrm{T}}^{\mathrm{miss}}$ is defined as the projection on the plane perpendicular to the beams of the negative vector sum of the momenta of all PF candidate particles in an event [48]. Its magnitude is referred to as $E_{\mathrm{T}}^{\mathrm{miss}}$.

5   Event selections

The kinematical selection criteria used to define the signal region, containing a sample of candidate signal events, as well as a number of control regions in data, are described below. The criteria are based on the physics objects defined by the event reconstruction algorithms described in Section 4.

5.1   Common preselection criteria

A number of beam- and detector-related effects, such as beam halo, reconstruction failures, spurious detector noise, or event misreconstruction due to detector inefficiencies, can lead to events with anomalous levels of activity. These events, which can exhibit large, non-physical values of $E_{\mathrm{T}}^{\mathrm{miss}}$, are rejected with high efficiency by applying a range of dedicated vetoes [48–50].

In order to suppress SM processes with genuine $E_{\mathrm{T}}^{\mathrm{miss}}$ from neutrinos, events containing an isolated electron or muon that satisfy $p_{\mathrm{T}} > 10$ GeV and $|\eta| < 2.5$ are vetoed. Events containing an isolated photon with $p_{\mathrm{T}} > 25$ GeV and $|\eta| < 2.5$ are also vetoed, in order to select only multijet final states. Furthermore, events containing a single isolated track satisfying $p_{\mathrm{T}} > 10$ GeV and $|\eta| < 2.5$ and vetoed in order to reduce the background contribution from final states containing hadronically-decaying tau leptons.

Each jet j_{i} is required to satisfy $p_{\mathrm{T}}^{j_{\mathrm{i}}} > 40$ GeV and $|\eta^{j_{\mathrm{i}}}| < 3$. The highest p_{T} jet in the event is required to satisfy the tighter requirements $p_{\mathrm{T}}^{j_1} > 100$ GeV and $|\eta^{j_1}| < 2.5$. The second highest p_{T} jet in the event is used to categorise events, as described in Section 5.2. If the jet satisfies $p_{\mathrm{T}}^{j_2} > 100$ GeV, then this category of events is labelled "symmetric" and targets primarily topologies resulting from pair-produced sparticles. If the jet satisfies $40 < p_{\mathrm{T}}^{j_1} < 100$ GeV or $p_{\mathrm{T}}^{j_2} < 40$ GeV, then these categories are labelled as, respectively, "asymmetric" or "monojet" topologies, which target primarily nearly mass-degenerate strongly produced models and weakly produced models.

The mass scale of the physics processes being probed is characterised by the scalar p_{T} sum of

Table 1: Summary of the event selection criteria and categorisation used to define the signal and control regions.

Common preselection	
E_T^{miss} cleaning	Filters related to beam and instrumental effects
Lepton/photon vetoes	$p_T > 10, 10, 25$ GeV for isolated tracks, leptons, photons (respectively) and $|\eta| < 2.5$
Jet j_i acceptance	Consider each jet j_i that satisfies $p_T^{j_i} > 40$ GeV and $|\eta^{j_i}| < 3$
Jet j_1 acceptance	$p_T^{j_1} > 100$ GeV and $|\eta^{j_1}| < 2.5$
Jet j_2 acceptance	$p_T^{j_2} < 40$ GeV (monojet), $40 < p_T^{j_2} < 100$ GeV (asymmetric), $p_T^{j_2} > 100$ GeV (symmetric)
Forward jet veto	Veto events containing jet satisfying $p_T > 40$ GeV and $|\eta| > 3$
Jets below threshold	$H_T^{miss}/E_T^{miss} < 1.25$
Energy sums	$H_T > 200$ GeV and $H_T^{miss} > 130$ GeV
Event categorisation	
n_{jet}	1 (monojet), 2, 3, 4, ≥ 5 (asymmetric), 2, 3, 4, ≥ 5 (symmetric)
n_b	0, 1, 2, ≥ 3 ($n_b \leq n_{jet}$)
H_T (GeV)	200, 250, 300, 350, 400, 500, 600, >800 GeV (bins can be dropped/merged *vs.* n_{jet}, Table 2)
Signal region (SR)	Preselection +
QCD multijet rejection	$\alpha_T > 0.65, 0.60, 0.55, 0.53, 0.52, 0.52, 0.52$ (mapped to H_T bins in range $200 < H_T < 800$ GeV)
QCD multijet rejection	$\Delta\phi_{min}^* > 0.5$ (for the region $H_T > 200$ GeV)
Control regions (CR)	Preselection +
Multijet-enriched	SR + $H_T^{miss}/E_T^{miss} > 1.25$ (inverted)
γ+jets	1γ with $p_T > 200$ GeV, $|\eta| < 1.45$, $\Delta R(\gamma, j_i) > 1.0$, $H_T > 400$ GeV, same α_T req. as SR
μ+jets	1μ with $p_T > 30$ GeV, $|\eta| < 2.1$, $I_{rel}^\mu < 0.1$, $\Delta R(\mu, j_i) > 0.5$, $30 < m_T(\vec{p}_T^\mu, \vec{p}_T^{miss}) < 125$ GeV
$\mu^\pm\mu^\mp$+jets	2μ with $p_T > 30$ GeV, $|\eta| < 2.1$, $I_{rel}^\mu < 0.1$, $\Delta R(\mu_{1,2}, j_i) > 0.5$, $|m_{\mu\mu} - m_Z| < 25$ GeV

the jets, defined as $H_T = \sum_{i=1}^{n_{jet}} p_T^{j_i}$, where n_{jet} is the number of jets within the experimental acceptance. An estimator for E_T^{miss} is given by the magnitude of the negative vector $\vec{p}_T$ sum of these jets, defined by $H_T^{miss} = |-\sum_{i=1}^{n_{jet}} \vec{p}_T^{j_i}|$. Events are vetoed if any jet satisfies $p_T > 40$ GeV and $|\eta| > 3$ in order to maintain the performance of the variable H_T^{miss} as an estimator of E_T^{miss}.

The dimensionless variable H_T^{miss}/E_T^{miss} is employed to deal with the rare circumstance in which events contain several jets with transverse momenta below the jet p_T thresholds but an appreciable p_T vector sum so as to contribute significantly to H_T^{miss} relative to E_T^{miss}, the latter of which is insensitive to jet p_T thresholds. This type of event topology can lead to a significant background contribution from multijet events. The requirement $H_T^{miss}/E_T^{miss} < 1.25$ suppresses contributions from multijet events in the signal region, defined below, while maintaining high efficiency for new-physics processes with genuine $\vec{p}_T^{miss}$. The requirement is imposed as part of the common preselection criteria in order to minimise systematic uncertainties associated with simulation mismodelling for this variable when estimating SM backgrounds using the control regions in data.

Significant jet activity and missing transverse momentum in the event is ensured by requiring $H_T > 200$ GeV and $H_T^{miss} > 130$ GeV, respectively. These requirements complete the common preselection criteria, summarised in Table 1, used to define a sample of all-jet events characterised by high activity and appreciable missing transverse momentum.

5.2 Event categorisation

Events selected by the common preselection criteria are categorised according to n_{jet}, the number of b-tagged jets n_b, and H_T. Nine categories in n_{jet} are employed: the monojet topology ($n_{jet} = 1$) and four n_{jet} bins (2, 3, 4, ≥ 5) for each of the asymmetric and symmetric topolo-

Table 2: Summary of the lower bounds of the first and final bins in H_T (the latter in parentheses) as a function of n_{jet} and n_b.

$n_{jet} \setminus n_b$	0	1	2	≥ 3
Monojet				
1	200 (600)	200 (500)	-	-
Asymmetric				
2	200 (600)	200 (500)	200 (400)	-
3	200 (600)	200 (600)	200 (500)	200 (300)
4	200 (600)	200 (600)	200 (600)	250 (400)
≥ 5	250 (600)	250 (600)	250 (600)	300 (500)
Symmetric				
2	200 (800)	200 (800)	200 (600)	-
3	200 (800)	250 (800)	250 (800)	- (250)
4	300 (800)	300 (800)	300 (800)	300 (800)
≥ 5	350 (800)	350 (800)	350 (800)	350 (800)

gies. Events are also categorised by n_b (0, 1, 2, ≥ 3), where n_b is bounded from above by n_{jet}, resulting in 32 categories in terms of both n_{jet} and n_b. For each (n_{jet},n_b) category, events are binned according to H_T: four 50 GeV bins at low jet activity in the range $200 < H_T < 400$ GeV, two 100 GeV bins in the range $400 < H_T < 600$ GeV, one bin covering the region $600 < H_T < 800$ GeV, and a final open bin for $H_T > 800$ GeV. These categorisations are summarised in Table 1. The H_T binning scheme is adapted independently per (n_{jet},n_b) category by removing or merging bins to satisfy a threshold on the minimum number of data events in the control regions, which are used to estimate SM backgrounds, provide checks, and validate assumptions within the methods. The lower bounds of the first and final (open) bins in H_T are summarised in Table 2. In summary, the search employs a categorisation scheme for events that results in 191 bins, defined in terms of n_{jet}, n_b, and H_T.

5.3   Signal region

For events satisfying the common preselection criteria described above, the multijet background dominates over all other SM backgrounds. Several variables are employed to reduce the multijet contribution to a negligible level with respect to other SM backgrounds.

The dimensionless kinematic variable α_T [12, 18] is used to provide discrimination against multijet events that do not contain significant $\vec{p}_T^{\,miss}$ or that contain large $\vec{p}_T^{\,miss}$ only because of transverse momentum mismeasurements, while retaining sensitivity to new-physics events with significant $\vec{p}_T^{\,miss}$. The α_T variable depends solely on the transverse component of jet four-momenta and is intrinsically robust against the presence of jet energy mismeasurements in multijet systems. For events containing only two jets, α_T is defined as $\alpha_T = E_T^{j_2}/M_T$, where $E_T = E\sin\theta$, with E the energy of the jet and θ its polar angle with respect to the beam axis, $E_T^{j_2}$ is the transverse energy of the jet with smaller E_T, and M_T is the transverse mass of the dijet system, defined as:

$$M_T = \sqrt{\left(\sum_{i=1}^{2} E_T^{j_i}\right)^2 - \left(\sum_{i=1}^{2} p_x^{j_i}\right)^2 - \left(\sum_{i=1}^{2} p_y^{j_i}\right)^2}, \tag{1}$$

where $E_T^{j_i}$, $p_x^{j_i}$, and $p_y^{j_i}$ are, respectively, the transverse energy and x or y components of the transverse momentum of jet j_i.

For a perfectly measured dijet event with $E_T^{j_1} = E_T^{j_2}$ and the jets in the back-to-back configuration ($\Delta\phi = \pi$), and in the limit in which the momentum of each jet is large compared with its mass, the value of α_T is 0.5. For an imbalance in the E_T of back-to-back jets, α_T is reduced to a value < 0.5, which gives the variable its intrinsic robustness. Values significantly greater than 0.5 are observed when the two jets are not back-to-back and recoil against significant, genuine $\vec{p}_T^{\mathrm{miss}}$ from weakly interacting particles that escape the detector, such as neutrinos.

The definition of the α_T variable can be generalised for events with more than two jets [12]. The mass scale for any process is characterised through the scalar E_T sum of jets, defined as $S_T = \sum_{i=1}^{N_{\mathrm{jet}}} |\vec{E}_T^{\,j_i}|$, where N_{jet} is the number of jets with E_T above a predefined threshold. The estimator for $\vec{p}_T^{\mathrm{miss}}$ is H_T^{miss}. For events with three or more jets, a pseudo-dijet system is formed by combining the jets in the event into two pseudo-jets. The total S_T for each of the two pseudo-jets is given by the scalar E_T sum of its contributing jets. The combination chosen is the one that minimises ΔS_T, defined as the difference between the two pseudo-jets. This clustering criterion assumes a balanced-event hypothesis, which provides the best separation between SM multijet events and events with genuine $\vec{p}_T^{\mathrm{miss}}$. The α_T definition can be generalised to:

$$\alpha_T = \frac{1}{2}\frac{S_T - \Delta S_T}{\sqrt{(S_T)^2 - (H_T^{\mathrm{miss}})^2}}. \tag{2}$$

When jet energies are mismeasured, or there are neutrinos from heavy-flavour quark decays, the magnitude of H_T^{miss} and ΔS_T are highly correlated. This correlation is much weaker for R-parity-conserving SUSY events, where each of the two decay chains produces an undetected LSP.

Multijet events populate the region $\alpha_T < 0.5$ and the α_T distribution is characterised by a sharp edge at 0.5, beyond which the multijet event yield falls by several orders of magnitude. Multijet events with extremely rare but large stochastic fluctuations in the calorimetric measurements of jet energies can lead to values of α_T slightly above 0.5. The edge at 0.5 sharpens with increasing H_T for multijet events, primarily due to a corresponding increase in the average jet energy and a consequent improvement in jet energy resolution.

For events containing at least two jets, thresholds on the minimum allowed α_T values are applied independent of n_{jet} and n_b but dependent on H_T, for events that satisfy $200 < H_T < 800\,\mathrm{GeV}$. The α_T thresholds vary between 0.65 to 0.52 for, respectively, the regions $200 < H_T < 250\,\mathrm{GeV}$ and $400 < H_T < 800\,\mathrm{GeV}$. No requirement on α_T is made for the region $H_T > 800\,\mathrm{GeV}$. The thresholds employed are summarised in Table 1. The α_T thresholds are motivated both by the trigger conditions used to record the candidate signal events, described below, and by simulation-based studies and data-derived estimates of the multijet background.

A further variable considers the minimum azimuthal separation between a jet and the negative vector $\vec{p}_T$ sum derived from all other jets in the event [12],

$$\Delta\phi_{\min}^* = \min_{\forall\, j_k \in n_{\mathrm{jet}}} \Delta\phi\left(\vec{p}_T^{\,j_k}, -\sum_{j_i=1}^{n_{\mathrm{jet}}} \vec{p}_T^{\,j_i} + \vec{p}_T^{\,j_k}\right). \tag{3}$$

This variable discriminates between final states with genuine $\vec{p}_T^{\mathrm{miss}}$, e.g. from the leptonic decay of the W boson, and energetic multijet events that have significant $\vec{p}_T^{\mathrm{miss}}$ through jet energy mismeasurements or through the production of neutrinos, collinear with the axis of a jet, from semileptonic heavy-flavour decays. Multijet events populate the region $\Delta\phi_{\min}^* < 0.5$, with

the multijet distribution peaking at a value of zero and falling approximately exponentially over five orders of magnitude to the event level at a value of $\Delta\phi^*_{\min} \approx 0.5$, which is close to the radius parameter value of 0.4 used by the anti-k_t jet clustering algorithm. Events with a genuine source of $\vec{p}^{\,\mathrm{miss}}_T$ exhibit a long tail in $\Delta\phi^*_{\min}$ with values as large as π. The $\Delta\phi^*_{\min}$ variable provides comparable or improved performance in terms of discrimination according to a simple signal-to-background metric for a wide range of signal models with respect to more widely used variables such as:

$$\Delta\phi_{\min} = \min_{\forall\, j_k \in n_{\mathrm{jet}}} \Delta\phi(\vec{p}^{\,j_k}_T, -\sum_{j_i=1}^{n_{\mathrm{jet}}} \vec{p}^{\,j_i}_T). \tag{4}$$

The requirement $\Delta\phi^*_{\min} > 0.5$ is sufficient to effectively suppress the multijet background to a negligible level while maintaining high efficency to new-physics signatures. The combined rejection power of the α_T and $\Delta\phi^*_{\min}$ requirements for the region $200 < H_T < 800\,\mathrm{GeV}$ are sufficient to suppress multijet events to the few percent level with respect to all other SM backgrounds in all H_T bins for all event categories of the signal region. For the region $H_T > 800\,\mathrm{GeV}$, a similar control of the multijet background is achieved solely with the $\Delta\phi^*_{\min} > 0.5$ requirement.
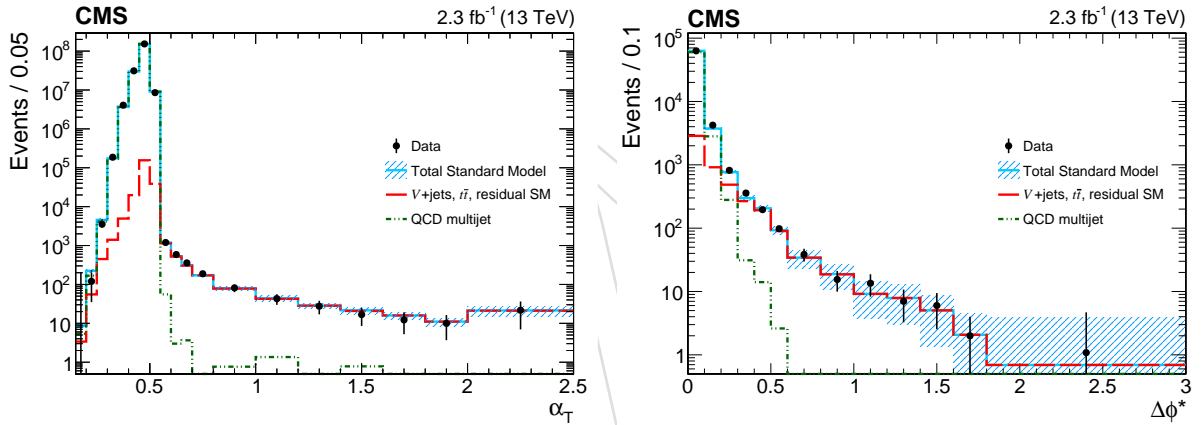

Figure 1: (Left) The α_T distribution observed in data for events that are recorded with unbiased trigger conditions and satisfy either the common preselection criteria and $\alpha_T < 0.55$, or the full signal region selection criteria and $\alpha_T > 0.55$, as well as the additional requirement $H_T > 300\,\mathrm{GeV}$. (Right) The $\Delta\phi^*_{\min}$ distribution observed in data for events that are recorded with unbiased trigger conditions and satisfy the full signal region selection criteria for the region $H_T > 800\,\mathrm{GeV}$. The distributions for the QCD multijet backgrounds are determined from simulation while all other SM backgrounds are estimated using a μ + jets data control sample.

Figure 1 illustrates the performance of the α_T and $\Delta\phi^*_{\min}$ variables, by showing their distributions observed in data for events that satisfy all other signal region selection criteria, as defined in Table 1, and additional requirements on H_T. In the case of the α_T distribution, the events that satisfy $\alpha_T < 0.55$ must only fulfill the common preselection criteria defined in Table 1, no H^{miss}_T requirement is made, and the events are recorded with an unbiased set of trigger H_T conditions. The contribution from multijet events is observed to fall by five orders of magnitude for both variables.

The aforementioned requirements complete the event selection criteria for the signal region. The α_T and $\Delta\phi^*_{\min}$ requirements, in conjunction with the common preselection requirements

$H_T^{miss} > 130$ GeV and $H_T^{miss}/E_T^{miss} < 1.25$, provide strong rejection power against contributions from multijet events. Finally, a modification to the $\Delta\phi^*_{min}$ variable, which considers soft jets with $p_T > 25$ GeV and is henceforth labeled $\Delta\phi^{*25}_{min}$, is used as a control variable in data to identify multijet contributions arising from instrumental effects, such as inefficient detector elements or detector noise. The axis of any jet that satisfies $\Delta\phi^{*25}_{min} < 0.5$ is used to identify localised behaviour in the (η,ϕ) plane, which may be indicative of instrumental defects. No significant anomolies are observed in the sample of candidate signal events following the application of the dedicated vetoes mentioned in Section 5.1.

Signal candidate events are recorded with multiple jet-based trigger conditions that utilise calculations of H_T and α_T, and events are required to satisfy predetermined thresholds for both variables, as well as a threshold on the mean p_T of the two highest p_T jets. In addition, a trigger condition based solely on H_T is used to record candidate events for the region $H_T > 800$ GeV. A further trigger condition comprising the presence of significant H_T^{miss} and E_T^{miss} is used to record monojet events. The trigger-level jet energies are corrected to account for energy scale and pileup effects. The trigger strategy provides efficiencies at or near 100% for all bins in the signal region.

5.4 H_T^{miss} templates

Following the event selections described above, which provide a sample of signal candidate events with a negligible contribution from mulitjet events, further discriminating power is required to separate new-physics signatures from the remaining SM backgrounds, which are dominated by the production of $t\bar{t}$ or $W(\to \ell\nu)$+jets and $Z(\to \nu\bar{\nu})$+jets events. Given the characteristic signature of SUSY production at the LHC is a final state of multijets accompanied by large values of $\vec{p}_T^{miss}$ from the LSPs, the search exploits the use of the H_T^{miss} variable as an additional discriminant between new-physics and SM processes.

The search relies directly on simulation to provide an estimate of the expected distribution of events as a function of H_T^{miss} in each (n_{jet}, n_b, H_T) bin. The distributions are described by templates that are used by the likelihood function as a model for the data, details on which can be found in Section 7. The templates are extensively validated against data in multiple control regions, and these studies are used to establish the uncertainty in the simulation modelling of the H_T^{miss} variable. The effect of theoretical and experimental uncertainties on the H_T^{miss} distributions are also studied. Further details can be found in Sections 6.2.

5.5 Control regions

Four control regions in data are employed to estimate the background contributions from SM processes, which modify and expand on the common preselection criteria described above, according to the descriptions found below and summarised in Table 1.

The first control region comprises a multijet-enriched sample of events, and is defined by the signal region selection criteria and the inverted requirement $H_T^{miss}/E_T^{miss} > 1.25$. The events are recorded with the signal triggers described above, and the sample is used to estimate the multijet background in the signal region.

Three additional control regions are used to estimate background contributions from SM processes with final states containing genuine $\vec{p}_T^{miss}$, and are defined by inverting one of the photon or lepton vetoes to select samples of γ+jets, μ+jets, or $\mu\mu$+jets events. Additional kinematic requirements are employed to ensure the control samples are enriched in the same SM processes that contribute to background events in the signal region, and are depleted in contributions

from multijet production or a wide variety of SUSY models (i.e. so-called signal contamination). The samples are defined, and their events are identically categorised and binned, such that the kinematic properties of events in the control regions and the signal candidate events resemble as closely as possible one another, once the photon, muon, or dimuon system is ignored in the calculation of quantities such as H_T and $H_\mathrm{T}^\mathrm{miss}$. The selections are summarised in Table 1 and described below.

The γ+jets event sample is defined by the common preselection requirements, but the photon veto is inverted and each event is required to contain a single isolated photon, as defined in Section 4, that satisfies $p_\mathrm{T} > 200\,\mathrm{GeV}$ and $|\eta| < 1.45$ and well separated from each jet j_i in the event according to $\Delta R(\gamma, j_\mathrm{i}) > 1.0$. In addition, events must satisfy $H_\mathrm{T} > 400\,\mathrm{GeV}$, as well as the same H_T-dependent α_T requirements used to define the signal region. The events are recorded using a single-photon trigger condition and the selections result in a trigger efficiency of $\gtrsim$99%.

The μ+jets event sample is defined by the common preselection requirements, but the muon veto is inverted and each event is required to contain a single isolated muon, as defined in Section 4, that satisfies $p_\mathrm{T} > 30\,\mathrm{GeV}$ and $|\eta| < 2.1$ and well separated from each jet j_i in the event according to $\Delta R(\mu, j_\mathrm{i}) > 0.5$. The transverse mass formed by the tranvserve momenta of the muon and $\vec{p}_\mathrm{T}^\mathrm{miss}$ system must satisfy $30 < m_\mathrm{T} < 125\,\mathrm{GeV}$ to select a sample of events rich in W bosons, produced promptly or from the decay of top quarks. The $\mu\mu$+jets sample uses a similar set of selection criteria as the μ+jets sample, but specifically requires two oppositely charged isolated muons that both satisfy $p_\mathrm{T} > 30\,\mathrm{GeV}$ and $|\eta| < 2.1$ and are well separated from the jets in the event ($\Delta R(\mu_{1,2}, j_\mathrm{i}) > 0.5$). The muons are also required to have a dilepton invariant mass within a $\pm 25\,\mathrm{GeV}$ window around the nominal mass of the Z boson. For both the muon and dimuon samples, no requirement is made on α_T, in order to increase the statistical precision of the predictions from these samples. Both the μ+jets and $\mu\mu$+jets samples are recorded using a trigger that requires an isolated muon. The selection criteria of the μ+jets and $\mu\mu$+jets event samples are chosen so that the trigger is maximally efficient with values in the region, respectively, $\approx$90% and $\approx$99%.

6   Estimation of backgrounds

6.1   Multijets background

The signal region is defined in a manner to suppress the expected contribution from multijet production to the percent level with respect to the total expected background counts from other SM processes for all event categories, defined in terms of n_jet and n_b, and all bins, defined in H_T and $H_\mathrm{T}^\mathrm{miss}$. This is achieved primarily through the application of very tight requirements on the variables α_T and $\Delta\phi_\mathrm{min}^*$, as described in Section **??**, as well as the requirement $H_\mathrm{T}^\mathrm{miss} / E_\mathrm{T}^\mathrm{miss} <$ 1.25. In this section, we discuss these requirements further, and the estimate of the suppression of the multijet background.

The contamination from multijet events in the signal region is estimated using a multijet-enriched data sideband to the signal region, defined by the (inverted) requirement $H_\mathrm{T}^\mathrm{miss} / E_\mathrm{T}^\mathrm{miss} >$ 1.25. The observed counts in data are categorised according to n_jet and H_T and are corrected to account for contamination from vector boson and $t\bar{t}$ production, and residual contributions from other SM processes, which are estimated using the μ+jets control region with the method described in Section 6.2. The corrected data counts $\mathcal{N}^\mathrm{data}(n_\mathrm{jet}, H_\mathrm{T})$ are used to estimate the multijet background in the signal region $\mathcal{P}(n_\mathrm{jet}, H_\mathrm{T})$ through multiplication with the ratio $\mathcal{R}^\mathrm{QCD}(n_\mathrm{jet}, H_\mathrm{T})$ of multijet events that satisfy the requirement $H_\mathrm{T}^\mathrm{miss} / E_\mathrm{T}^\mathrm{miss} < 1.25$ to those that
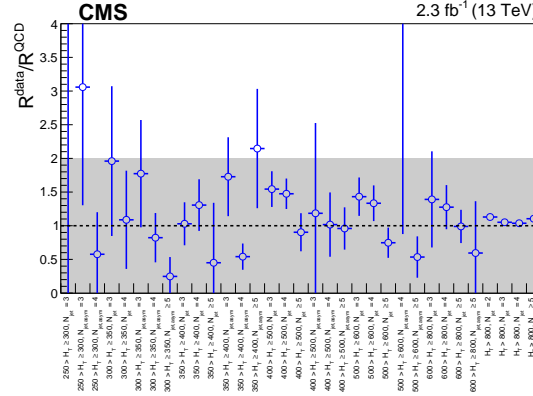
Figure 2: Validation of the ratio $\mathcal{R}^{\text{QCD}}$ determined from simulation in bins of n_{jet} and H_T by comparing with an equivalent ratio $\mathcal{R}^{\text{data}}$ constructed from data in a multijet-enriched sideband to the signal region. A value of unity is expected for the double ratio $\mathcal{R}^{\text{data}}/\mathcal{R}^{\text{QCD}}$, and the grey shaded band represents the assumed systematic uncertainty of 100% in $\mathcal{R}^{\text{QCD}}$.

fail, which is determined independently for events categorised according to n_{jet} and H_T from simulation. Finally, the differential distribution of $\mathcal{P}(n_{\text{jet}}, H_T)$ as a function of n_b and H_T^{miss} is described by the multiplier term $\mathcal{K}_{n_{\text{jet}}, H_T}(n_b, H_T^{\text{miss}})$, which is assumed to exhibit the same distribution as the nonmultijet backgrounds, as determined from simulation. Assuming i, j, k, and l are the bin indices for, respectively, n_{jet}, H_T, n_b, and H_T^{miss}:

$$\mathcal{P}(i,j,k,l) = \mathcal{N}^{\text{data}}(i,j)\,\mathcal{R}^{\text{QCD}}(i,j)\,\mathcal{K}_{i,j}(k,l). \tag{5}$$

The use of simulation to determine $\mathcal{R}^{\text{QCD}}(n_{\text{jet}}, H_T)$ is validated using a multijet-enriched data sideband defined by $\Delta\phi_{\text{min}}^* < 0.5$. The ratio $\mathcal{R}^{\text{data}}(n_{\text{jet}}, H_T)$ is constructed from data counts, corrected to account for contributions from nonmultijet processes, and compared with $\mathcal{R}^{\text{QCD}}(n_{\text{jet}}, H_T)$, determined from simulation, through the double ratio $\mathcal{R}^{\text{data}}/\mathcal{R}^{\text{QCD}}$, as shown in Fig. 2. The double ratios are observed to be close to, or statistically compatible with, unity across the full phase space of the signal region, including the bins at high H_T, which exhibit the highest statistical precision. An uncertainty of 100% in $\mathcal{R}^{\text{QCD}}$ is assumed to adequately cover the observed level of agreement for the full signal region phase space.

Finally, data control variables, such as $\Delta\phi_{\text{min}}^{*\,25}$, are inspected for localised populations in (η, ϕ)-space to provide confidence that any multijet contamination due to instrumental effects is negligible.

6.2 Backgrounds with genuine E_T^{miss}

Following the suppression of multijet events through the use of the α_T and $\Delta\phi_{\text{min}}^*$ variables, the dominant nonmultijet backgrounds involve SM processes that produce high-p_T neutrinos in the final state. In events with few jets or few b quark jets, the associated production of W or Z bosons and jets, with the decays $W^\pm \to \ell\nu$ ($\ell = $ e, μ, τ) or $Z \to \nu\bar{\nu}$, dominate the background counts. For W boson decays that yield a muon or electron (possibly originating from leptonic τ decays), the background arises when the event containing the μ or e is not rejected by the lepton vetoes. Background also arises when the τ lepton decays to hadrons, identified as a jet, and neutrinos. The veto of events containing at least one isolated track is efficient at further suppressing these backgrounds, including those from single-prong τ-lepton decays. At higher

491   jet or b quark jet multiplicities, single top and $t\bar{t}$ production, followed by semileptonic top
492   quark decay, also become an important source of background.

493   The method to estimate the nonmultijet backgrounds in the signal region relies on the use of
494   transfer factors determined from simulation that are constructed per bin (in terms of n_{jet}, n_{b},
495   and H_{T}) per control region. Each transfer factor is defined as the ratio of the expected yields
496   in the same (n_{jet}, n_{b}, H_{T}) bins of the signal region $\mathcal{N}_{\text{MC}}^{\text{SR}}$ and one of the control regions $\mathcal{N}_{\text{MC}}^{\text{CR}}$.
497   The transfer factors are used to extrapolate from the event yields observed in each bin of a data
498   control sample $\mathcal{N}_{\text{data}}^{\text{CR}}$ to provide an estimate for the background, intergrated over $H_{\text{T}}^{\text{miss}}$, from
499   a particular SM process or processes in the corresponding bin of the signal region $\mathcal{N}_{\text{data}}^{\text{SR}}$. The
500   superscript SR or CR refers to, respectively, the process or processes being estimated and one of
501   the μ+jets, $\mu\mu$+jets, and γ+jets control regions, described in Section 5.5. The subscript refers
502   to whether the counts are obtained from data, simulation ("MC") or an estimate ("pred").

503   The method aims to minimise the effects of simulation mismodelling, as many systematic bi-
504   ases in the simulation are expected to largely cancel in the transfer factors, given that the events
505   in any given (n_{jet}, n_{b}, H_{T}) bin of the control regions closely mirror those in the corresponding
506   bin in the signal region, in terms of the event scale and topology, the kinematical phase, and the
507   relative background compositions. In short, minimal extrapolations are made. Uncertainties in
508   the transfers factors are determined from a data-derived approach, described below.

509   Three independent estimates of the irreducible background of $Z \to \nu\bar{\nu}$ + jets events are deter-
510   mined from the γ+jets, $\mu\mu$+jets, amd μ+jets data control samples. The γ+jets and $Z \to \mu\mu$ +
511   jets processes have similar kinematic properties when the photon or muons are ignored [51],
512   albeit different acceptances. In addition, the γ+jets process has a larger production cross sec-
513   tion than $Z \to \nu\bar{\nu}$ + jets events. The μ+jets data sample is used to provide an estimate for both
514   the $Z \to \nu\bar{\nu}$ + jets background, as well as the other dominant SM processes, $t\bar{t}$ and W boson
515   production (labelled collectively as W/$t\bar{t}$). Residual contributions from all other SM relevant
516   processes, such as single-top-quark, diboson, and Drell-Yan production, are also included as
517   part of the W/$t\bar{t}$ estimate from the μ+jets sample. The definition of the various transfer factors
518   used in the search are given below:

$$\mathcal{N}_{\text{pred}}^{\text{W}/t\bar{t}} = \left(\frac{\mathcal{N}_{\text{MC}}^{\text{W}/t\bar{t}}}{\mathcal{N}_{\text{MC}}^{\mu+\text{jets}}} \right) \mathcal{N}_{\text{data}}^{\mu+\text{jets}} \tag{6}$$

$$\mathcal{N}_{\text{pred}}^{Z \to \nu\bar{\nu}} = \left(\frac{\mathcal{N}_{\text{MC}}^{Z \to \nu\bar{\nu}}}{\mathcal{N}_{\text{MC}}^{\mu+\text{jets}}} \right) \mathcal{N}_{\text{data}}^{\mu+\text{jets}} \tag{7}$$

$$\mathcal{N}_{\text{pred}}^{Z \to \nu\bar{\nu}} = \left(\frac{\mathcal{N}_{\text{MC}}^{Z \to \nu\bar{\nu}}}{\mathcal{N}_{\text{MC}}^{\mu\mu+\text{jets}}} \right) \mathcal{N}_{\text{data}}^{\mu\mu+\text{jets}} \tag{8}$$

$$\mathcal{N}_{\text{pred}}^{Z \to \nu\bar{\nu}} = \left(\frac{\mathcal{N}_{\text{MC}}^{Z \to \nu\bar{\nu}}}{\mathcal{N}_{\text{MC}}^{\gamma+\text{jets}}} \right) \mathcal{N}_{\text{data}}^{\gamma+\text{jets}} \tag{9}$$

519   The likelihood function, described in Section 7, encodes the estimate via the transfer factors of
520   the W/$t\bar{t}$ background, as well as the three independent estimates of the $Z \to \nu\bar{\nu}$ background,
521   which are considered simultaneously.

522   Several sources of uncertainty in the transfer factors are evaluated. The most relevant effects
523   are discussed below, and generally fall into one of two categories. The first category concerns
524   uncertainties in "scale factor" corrections applied to simulation, which are determined using

Table 3: Systematic uncertainties (percent) in the transfer factors used in the method to estimate the SM backgrounds with genuine $\vec{p}_T^{\text{miss}}$ in the signal region. The quoted ranges provide representative values of the observed variations as a function of n_{jet} and H_T.

Systematic	Uncertainty in transfer factor [%]			
source	μ+jets $\Rightarrow$ t$\bar{\text{t}}$/W	μ+jets $\Rightarrow$ Z$\rightarrow\nu\bar{\nu}$	$\mu\mu$+jets $\Rightarrow$ Z$\rightarrow\nu\bar{\nu}$	γ+jets $\Rightarrow$ Z$\rightarrow\nu\bar{\nu}$
Scale factors (applied to simulation):				
Jet energy scale	$< 15\%$	$< 15\%$	$< 10\%$	$< 15\%$
b-tag eff. mistag	$< 5\%$	$< 5\%$	$< 2\%$	$< 2\%$
Lepton SFs	$2-5\%$	$2-5\%$	$2-5\%$	$-$
Pileup	$< 10\%$	$< 6\%$	$< 4\%$	$< 3\%$
Top quark p_T	$< 5\%$	$< 20\%$	$< 4\%$	$-$
Closure tests:				
W/Z ratio	$-$	$10-30\%$	$-$	$-$
Z/γ ratio	$-$	$-$	$-$	$10-30\%$
W/t$\bar{\text{t}}$ composition	$10-100\%$	$-$	$-$	$-$
W polarisation	$5-50\%$	$5-50\%$	$-$	$-$
α_T / $\Delta\phi_{\text{min}}^*$	$5-80\%$	$5-80\%$	$50-80\%$	$-$

525 inclusive data samples that are defined by loose selection criteria, to account for the mismod-
526 elling of theoretical and experimental parameters. The second category concerns "closure tests"
527 in data that probe various aspects of the accuracy of the simulation to model correctly the trans-
528 fer factors in the phase space of this search.

529 The uncertainties in the transfer factors are studied for variations in scale factors related to: the
530 jet energy scale (that result in changes as large as $\sim15\%$), the efficiency and misidentification
531 probability of b quark jets (up to 5%), and the efficiency to identify well-reconstructed, isolated
532 leptons (up to $\sim5\%$). A 5% uncertainty in the minimum bias cross section, $\sigma_{\text{MB}} = 69.0 \pm 3.5$ mb,
533 is assumed and propagated through to the reweighting procedure to account for differences be-
534 tween the simulated and data-derived measurements of the pileup distributions, which results
535 in changes of up to $\sim10\%$. The modelling of the transverse momentum of top quarks (p_T^t) is
536 evaluated by comparing the simulated and measured p_T spectra of reconstructed top objects in
537 t$\bar{\text{t}}$ events, using the technique described in Ref. []. Simulated events are reweighted according
538 to scale factors that decrease from a value of ~1.2 to ~0.7, with uncertainties of ~0.1, within
539 the range $0 < p_T^t < 400$ GeV. The resulting change in the transfer factors is as large as $\sim20\%$.
540 These uncertainties, resulting from variations in scale factors, are summarised in Table 3, along
541 with representative magnitudes. Each source of uncertainty is assumed to vary with a fully
542 correlated behaviour across the full phase space of the signal and control regions.

543 The second category of sources of uncertainty are determined from sets of "closure tests" based
544 on data control samples [15]. Each set uses the observed event counts in up to eight bins
545 in H_T for each of the nine n_{jet} event categories in one of the three independent data control
546 regions, along with the corresponding transfer factors determined from simulation, to obtain
547 a prediction, $\mathcal{N}^{\text{pred}}(n_{\text{jet}}, H_T)$, of the observed yields, $\mathcal{N}^{\text{obs}}(n_{\text{jet}}, H_T)$, in another control sample
548 (or, in one case, n_b event category).

549 Each set of tests is designed to target a specific (potential) source of bias in the simulation mod-
550 elling that may introduce an n_{jet}- or H_T-dependent source of systematic bias in the transfer
551 factors [15]. Several sets of tests are performed. The Z/γ ratio determined from simulation
552 is tested against the same ratio measured using Z($\rightarrow\mu\mu$)+jets events and the γ+jets sample.
553 The W/Z ratio is also probed using the μ+jets and $\mu\mu$+jets samples. A further set probes
554 the modelling of the relative composition between W($\rightarrow\ell\nu$)+jets and t$\bar{\text{t}}$ events using μ+jets

555 events containing exactly zero or one more b-tagged jets, which represents a larger extrapola-
556 tion in relative composition than used in the search. The effects of W polarisation are probed by
557 using μ+jets events with a positively charged muon to predict those containing a negatively
558 charged muon. Finally, the accuracy of the modelling of the efficiencies of the α_T and $\Delta\phi^*_{min}$
559 requirements are estimated using the μ+jets sample.

560 For each set of tests, the level of closure, $(\mathcal{N}^{obs} - \mathcal{N}^{pred})/\mathcal{N}^{obs}$, which considers only statistical
561 uncertainties, is inspected to ensure no statistically significant biases are observed as a func-
562 tion of the nine n_{jet} categories or the eight H_T bins. In the absence of such a bias, the level of
563 closure is recomputed by integrating over either all monojet and asymmetric n_{jet} categories, or
564 the symmetric n_{jet} categories. The level of closure and its statistical uncertainty are combined
565 in quadrature to determine additional contributions to the uncertainties in the transfer factors.
566 These uncertainties are considered to be fully correlated between the monojet and asymmet-
567 ric n_{jet} categories or the symmetric n_{jet} categories, and fully uncorrelated between these two
568 regions in n_{jet} and H_T bins. If the closure tests use the $\mu\mu$+jets sample, the level of closure
569 is determined by additionally integrating over pairs of adjacent H_T bins. These uncertainties,
570 derived from the closure tests in data, are summarised in Table 3, along with representative
571 magnitudes. These uncertainties are the dominant contribution to the total, due to the limited
572 number of events in the data control regions.

573 As introduced in Section 5.4, templates are derived from simulation to predict the background
574 counts in the H_T^{miss} dimension. The uncertainties in the transfer factors are used to constrain
575 the normalisation of the H_T^{miss} templates. The uncertainties in the H_T^{miss} shape are discussed
576 below.

577 The accuracy to which the simulation describes the H_T^{miss} distributions is evaluated with re-
578 spect to data, in each (n_{jet}, n_b, H_T) bin in each of the μ+jets, $\mu\mu$+jets, and γ+jets data control
579 regions. The level of agreement between data and simulation as a function of H_T^{miss} is param-
580 eterised using an orthogonal first-order polynomial, $f(x) = p_0 + p_1(\bar{x} - x)$, and described by
581 two uncorrelated parameters, p_0 and p_1. A binned likelihood fit is performed in each $(n_{jet}, n_b,$
582 $H_T)$ bin of each control region, and the best fit value p_1 and its uncertainty is used to determine
583 the presence of biases dependent on H_T^{miss}. The pull of p_1 from a value of zero is defined as the
584 best fit value over its standard deviation, considering only statistical uncertainties associated
585 with the finite size of the data and simulated samples.

586 The lower bound of the final (open) bin in H_T^{miss} is not more than 800 GeV and is bounded from
587 above by the upper bound of the H_T bin in question. The lower bound of the final H_T^{miss} bin is
588 merged with lower bins if fewer than ten events in the data control regions are observed. If a
589 bin in (n_{jet}, n_b, H_T) contains fewer than ten events, the H_T^{miss} template is not used. The merging
590 of bins is typically only relevant for event categories that satisfy $n_b \geq 2$.

591 The presence or otherwise of systematic biases is evaluated at a statistical level, by considering
592 the distribution of pulls obtained from each control region, which are consistent with statistical
593 fluctuations, with no indication of trends across the full phase space of each control region. The
594 p-values obtained from the fits are uniformly distributed.

595 The uncertainty in the H_T^{miss} modelling is extracted under the hypothesis of no bias. This is
596 done using the maximum likelihood (ML) values of the fit parameters to determine the statisti-
597 cal precision to which this hypothesis can be confirmed. The quadrature sum of the ML value
598 and its uncertainty for p_1 from each fit is used to define alternative templates that represent
599 $\pm 1\sigma$ variations to the nominal H_T^{miss} template. These alternative templates are encoded in the
600 likelihood function, as described in Section 7. The observed variations are compatible with the

expected values obtained from studies relying only on simulated event samples. The uncertainties in the final H_T^{miss} bin of the templates depend on the event category and H_T bin, but are typically found to be in the range ~10–100%.

The effect on the H_T^{miss} templates is determined under $\pm 1\sigma$ variations in the jet energy scale, the efficiency and misidentification probability of b quark jets, the efficiency to identify well-reconstructed, isolated leptons, the pileup reweighting, and the modelling in the top quark transverse momentum. These effects are easily covered by the data-derived uncertainties, described above, across the full phase space of the control regions, which mirror closely that of the signal region.

7 Results

A model of the observations in all data samples, described by a likelihood function, is used to obtain a consistent prediction of the SM backgrounds, and to test for the presence of new-physics signals if the signal region is included in the maximum-likelihood fit. The observation in each bin defined by the n_{jet}, n_b, H_T, and H_T^{miss} variables is modelled as a Poisson-distributed variable around the SM expectation and a potential signal contribution (assumed to be zero in the following discussion), where the SM expectation is the sum over the estimated contributions from all background processes according to the methods described in Section 6.

The non-multijet backgrounds, which comprise the $W(\to \ell\nu)$+jets and $t\bar{t}$+jets ("lost lepton") backgrounds, the residual contributions from other processes, such as single top, diboson, and Drell-Yan production, and the irreducible $Z(\to \nu\bar{\nu})$+jets background, are related to the expected yields in the μ+jets, $\mu\mu$+jets, and γ+jets control samples via the transfer factors derived from simulation, as described in Section 5.5. Estimates of the contribution from multijet events in the signal region is determined according to the method described in Section 6.1, and is included in the likelihood function.

The systematic uncertainties summarised in Table 3 are accommodated in the likelihood function through the use of nuisance parameters, the measurements of which are assumed to follow a log-normal distribution. Alternative templates are used to describe the uncertainties in the modelling of the H_T^{miss} variable. A vertical template morphing scheme [52] is used to interpolate between the nominal and alternative H_T^{miss} templates. A nuisance parameter controls the interpolation, which is gaussian distributed with a mean of zero and a standard deviation of one, where ± 1 corresponds to the alternative templates for a $\pm 1\sigma$ variation in the uncertainty. Each template is interpolated quadratically between $\pm 1\sigma$, and a linear extrapolation is employed beyond these bounds.

The "pre-fit" result of this search, which considers the observations in the control regions only, is summarised in Figs. 3, 4, and 5 for, respectively, the monojet, asymmetric, and symmetric topologies. This result is based on an estimate of the $Z(\to \nu\bar{\nu})$+jets background using observations in multiple control regions as described by the likelihood function, maximised over all fit parameters. The figures also show the significance of deviations observed in data with respect to the "pre-fit" SM expectations, expressed in terms of the total uncertainty in the SM expectations. Figures 3, 4, and 5 also summarise the pulls from the "post-fit" result, which is based on a maximum-likelihood fit to observations in the signal region as well as the control regions. No significant tension is observed between the data and SM expectations in the signal region (and control regions), and the data are well described by the background-only hypothesis. A saturated likelihood model [] is used as a goodness-of-fit test to determine the compatibility of the observed yields with the expectations from only SM processes (i.e. the background-only
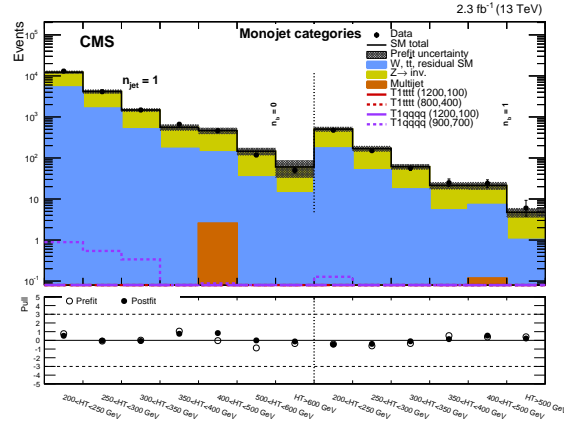
Figure 3: (Top panel) Event yields observed in data (solid circles) and "pre-fit" SM expectations with their associated uncertainties (black histogram with shaded band), integrated over H_T^{miss}, as a function of n_b, and H_T for the monojet category ($n_{jet} = 1$) in the signal region. For illustration only, the expectations for four benchmark models (defined in the text) are superimposed on the SM-only expectations. (Bottom panel). The significance of deviations observed in data with respect to both the "pre-fit" (open circles) and "post-fit" (closed circles) SM expectations, expressed in terms of the total uncertainty in the SM expectations.

hypothesis). A p-value of 0.20 is observed for the fit over the full signal region, and p-values in the range 0.04–1.00 and consistent with a uniform distribution when considering events categorised according to n_{jet}.

8   Interpretations

8.1   Specification for simplified models

The results of the search are used to constrain simplified supersymmetric models [53–55]. Each model assumes the pair production of gluinos or squarks and their subsequent prompt decays to SM particles and the LSP ($\widetilde{\chi}_1^0$) with a 100% branching ratio (unless indicated otherwise). The gluino decays contain intermediate on-shell sparticle states (such as the top squark, $\widetilde{t}$, or the chargino, $\widetilde{\chi}_1^\pm$) for a subset of the models. All other sparticles are assumed to be too heavy ($m_{\widetilde{g}}/m_{\widetilde{q}} = 10$ TeV) to be produced directly. Three-body decays of gluinos are assumed to occur via off-shell squarks of light or heavy flavour. All SM particles with a finite lifetime, such as the W boson, are assumed to decay naturally.

Fifteen unique production and decay modes are considered, which yield a range of topologies and final states (with only the all-jet final state considered in this search). Scans in the gluino or squark ($m_{\widetilde{g}}/m_{\widetilde{q}}$) and LSP ($m_{\widetilde{\chi}_1^0}$) mass parameter space are performed for each model. Each class of simplified model is identified by a label that indicates the topology and final state. Table 4 summarises the production and decay modes, as well as any additional assumptions that define each simplified model. The models can be categorised according to the following descriptions: the gluino-mediated and direct production of light-flavour squarks; the gluino-mediated production of off-shell third-generation squarks; the "natural" gluino-mediated production of on-shell top squarks; and the direct production of on-shell third-generation squarks. In the case of direct pair production of light-flavour squarks, two different assumptions on the theory production cross section are made. For the "eightfold" scenario (`T2qq_8fold`), the scalar partners to left- and right-handed quarks of the u, d, s, and c flavours are assumed to be light

Figure 4: (Top panel) Event yields observed in data (solid circles) and "pre-fit" SM expectations with their associated uncertainties (black histogram with shaded band), integrated over H_T^{miss}, as a function of n_{jet}, n_b, and H_T for the "asymmetric" n_{jet} categories in the signal region. For illustration only, the expectations for four benchmark models (defined in the text) are superimposed on the SM-only expectations. (Bottom panel). The significance of deviations observed in data with respect to both the "pre-fit" (open circles) and "post-fit" (closed circles) SM expectations, expressed in terms of the total uncertainty in the SM expectations.

671 and degenerate in mass, with other squark states decoupled to a high mass. For the "onefold"
672 scenario (T2qq_1fold), only a single light squark is assumed to particate in the interaction and
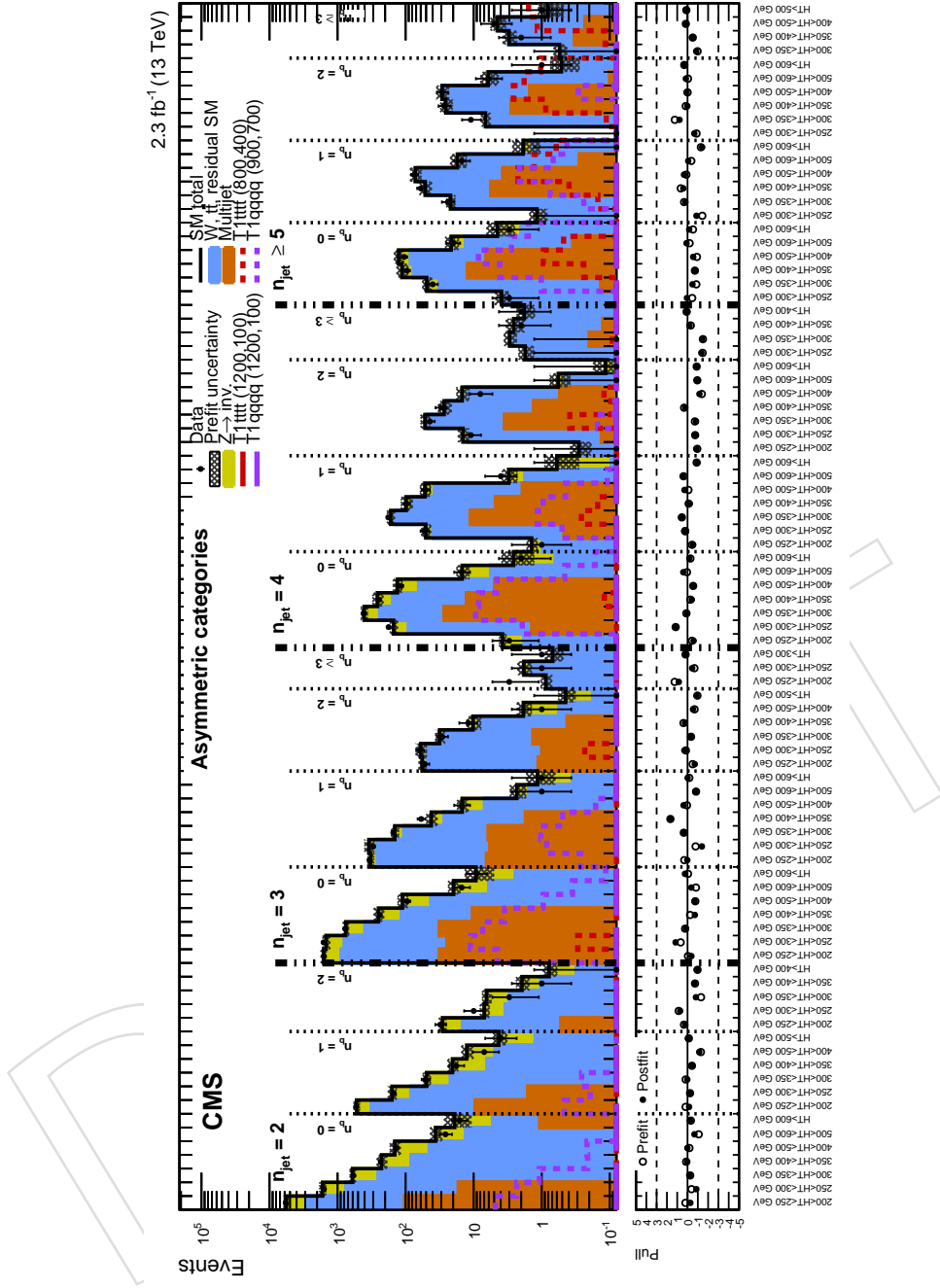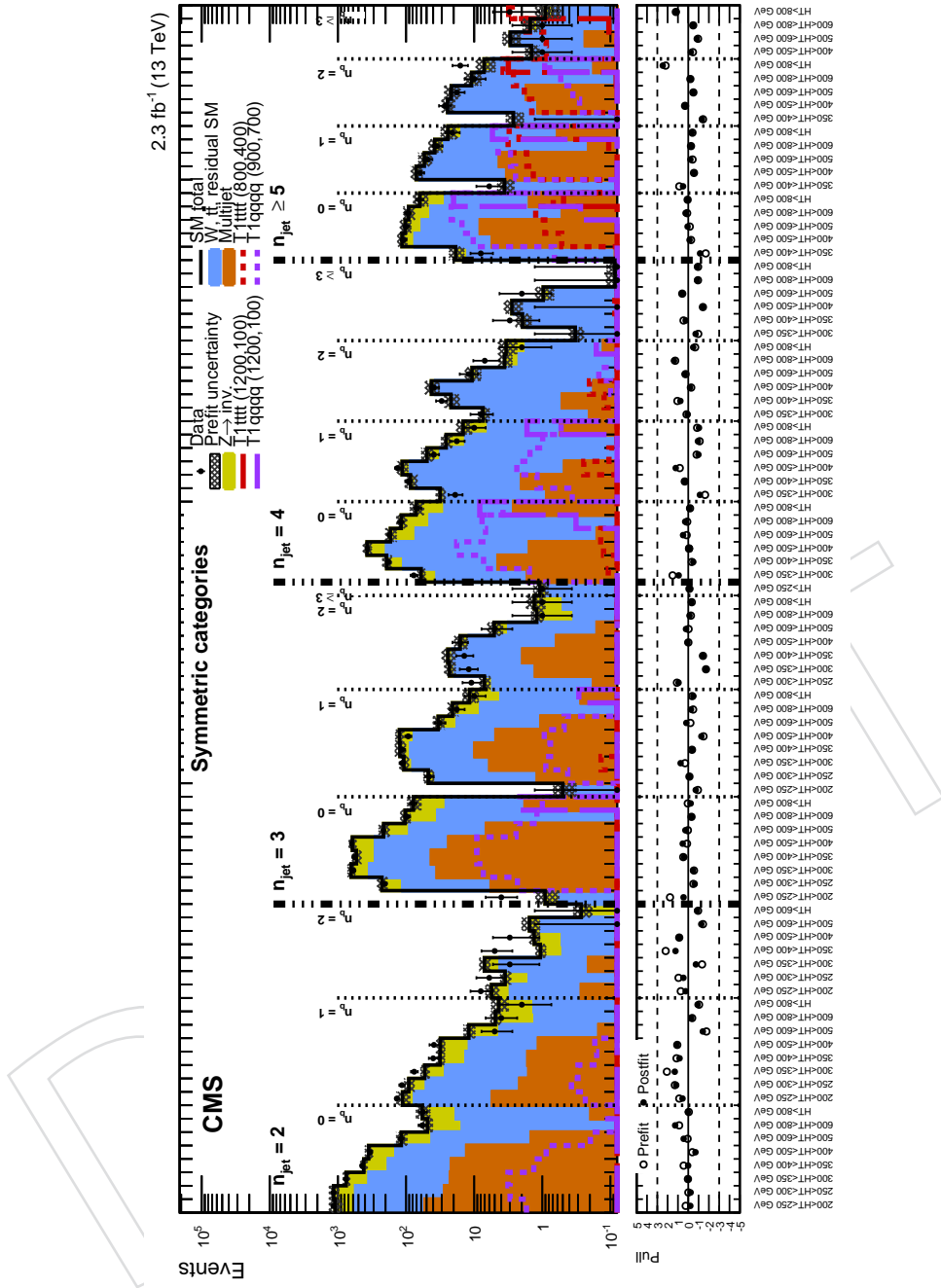
Figure 5: (Top panel) Event yields observed in data (solid circles) and "pre-fit" SM expectations with their associated uncertainties (black histogram with shaded band), integrated over H_T^{miss}, as a function of n_{jet}, n_b, and H_T for the "symmetric" n_{jet} categories in the signal region. For illustration only, the expectations for four benchmark models (defined in the text) are superimposed on the SM-only expectations. (Bottom panel). The significance of deviations observed in data with respect to both the "pre-fit" (open circles) and "post-fit" (closed circles) SM expectations, expressed in terms of the total uncertainty in the SM expectations.

673   all other squarks are decoupled to a high mass.

674   Under the background + signal hypothesis, and in the presence of a non-zero signal contribu-
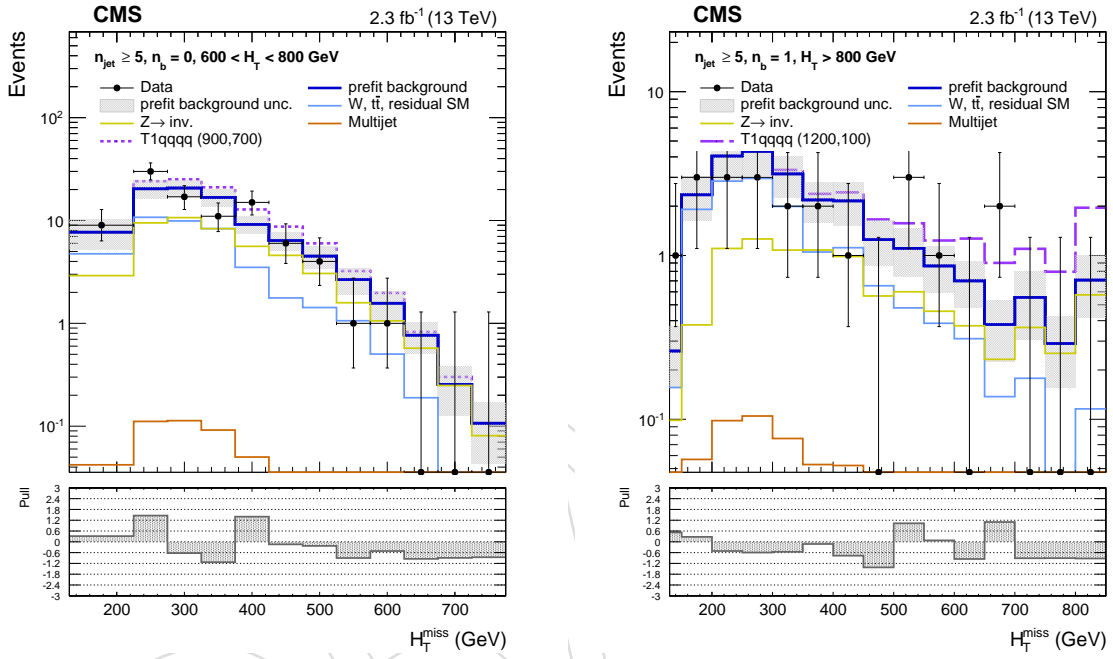
Figure 6: Event yields observed in data (solid circles) and "pre-fit" SM expectations with their associated uncertainties (blue histogram with shaded band) as a function of H_T^{miss} for events in the signal region that satisfy (Left) $n_{jet} \geq 5$, $n_b = 0$, $600 < H_T < 800\,\text{GeV}$ or (Right) $n_{jet} \geq 5$, $n_b = 1$, $H_T > 800\,\text{GeV}$. For illustration only, the expectations for a benchmark model (defined in the text) are superimposed on the SM-only expectations. The bottom panels indicate the significance of deviations observed in data with respect to both the "pre-fit" SM expectations, expressed in terms of the total uncertainty in the SM expectations.

Table 4: A summary of the simplified supersymmetric models used to interpret the results of this search. All on-shell sparticles in the decay are stated.

Topology	Fig.	Decay	Additional assumptions
Gluino-mediated and direct production of light-flavour squarks			
T1qqqq	$pp \to \widetilde{g}\widetilde{g}$	$\widetilde{g} \to \overline{q}q\widetilde{\chi}_1^0$	–
T2qq_8fold	$pp \to \widetilde{q}\overline{\widetilde{q}}$	$\widetilde{q} \to q\widetilde{\chi}_1^0$	$m_{\widetilde{q}} = m_{\widetilde{q}_L} = m_{\widetilde{q}_R}, \widetilde{q} = \{\widetilde{u}, \widetilde{d}, \widetilde{s}, \widetilde{c}\}$
T2qq_1fold	$pp \to \widetilde{q}\overline{\widetilde{q}}$	$\widetilde{q} \to q\widetilde{\chi}_1^0$	$m_{\widetilde{q}(\widetilde{q} \neq \widetilde{u}_L)} \gg m_{\widetilde{u}_L}$
Gluino-mediated production of off-shell third-generation squarks			
T1bbbb	$pp \to \widetilde{g}\widetilde{g}$	$\widetilde{g} \to \overline{b}b\widetilde{\chi}_1^0$	–
T1tttt	$pp \to \widetilde{g}\widetilde{g}$	$\widetilde{g} \to \overline{t}t^* \to \overline{t}t\widetilde{\chi}_1^0$	–
T1ttbb	$pp \to \widetilde{g}\widetilde{g}$	$\widetilde{g} \to \overline{t}b\widetilde{\chi}_1^\pm \to \overline{t}bW^*\widetilde{\chi}_1^0$	$m_{\widetilde{\chi}_1^\pm} - m_{\widetilde{\chi}_1^0} = 5\,\text{GeV}$
Natural gluino-mediated production of on-shell top squarks			
T5tttt	$pp \to \widetilde{g}\widetilde{g}$	$\widetilde{g} \to \overline{t}\widetilde{t} \to \overline{t}t\widetilde{\chi}_1^0$	$m_{\widetilde{t}} - m_{\widetilde{\chi}_1^0} = 175\,\text{GeV}$
T5ttcc	$pp \to \widetilde{g}\widetilde{g}$	$\widetilde{g} \to \overline{t}\widetilde{t} \to \overline{t}c\widetilde{\chi}_1^0$	$m_{\widetilde{t}} - m_{\widetilde{\chi}_1^0} = 20\,\text{GeV}$
T5tttt_degen	$pp \to \widetilde{g}\widetilde{g}$	$\widetilde{g} \to \overline{t}\widetilde{t} \to \overline{t}bW^*\widetilde{\chi}_1^0$	$m_{\widetilde{t}} - m_{\widetilde{\chi}_1^0} = 20\,\text{GeV}$
Direct production of on-shell third-generation squarks			
T2bb	$pp \to \widetilde{b}\overline{\widetilde{b}}$	$\widetilde{b} \to b\widetilde{\chi}_1^0$	–
T2tb	$pp \to \widetilde{t}\overline{\widetilde{t}}$	$\widetilde{t} \to t\widetilde{\chi}_1^0 \text{ or } b\widetilde{\chi}_1^\pm \to bW^*\widetilde{\chi}_1^0$	$\mathcal{BR} = 50/50\%, m_{\widetilde{\chi}_1^\pm} - m_{\widetilde{\chi}_1^0} = 5\,\text{GeV}$
T2tt	$pp \to \widetilde{t}\overline{\widetilde{t}}$	$\widetilde{t} \to t\widetilde{\chi}_1^0$	–
T2cc	$pp \to \widetilde{t}\overline{\widetilde{t}}$	$\widetilde{t} \to c\widetilde{\chi}_1^0$	$10 < m_{\widetilde{t}} - m_{\widetilde{\chi}_1^0} < 80\,\text{GeV}$
T2tt_degen	$pp \to \widetilde{t}\overline{\widetilde{t}}$	$\widetilde{t} \to bW^*\widetilde{\chi}_1^0$	$10 < m_{\widetilde{t}} - m_{\widetilde{\chi}_1^0} < 80\,\text{GeV}$
T2tt_mixed	$pp \to \widetilde{t}\overline{\widetilde{t}}$	$\widetilde{t} \to c\widetilde{\chi}_1^0 \text{ or } bW^*\widetilde{\chi}_1^0$	$\mathcal{BR} = 50/50\%, 10 < m_{\widetilde{t}} - m_{\widetilde{\chi}_1^0} < 80\,\text{GeV}$

675 tion, a modified frequentist approach is used to determine upper limits at 95% confidence level
676 (CL) on the cross section, σ_{UL} (pb), to produce pairs of supersymmetric particles as a function
677 of the parent sparticle and the LSP masses. The potential contributions from a new-physics
678 signal to each of the signal and control regions are considered, even though the only significant
679 contribution occurs in the signal region and not the control region (i.e. signal contamination).
680 The approach is based on the one-sided (LHC-style) profile likelihood ratio as the test statistic,
681 the CL_s criterion [56, 57], and asymptotic formulae [58] are utilised to approximate the distribu-
682 tions of the test statistics under the SM background-only and signal + background hypotheses.

683 **8.2 Acceptances and uncertainties**

684 The experimental acceptance times efficiency ($\mathcal{A} \times \varepsilon$) and its uncertainty are evaluated indepen-
685 dently for each model as a function of ($m_{\text{SUSY}}, m_{\text{LSP}}$). Table 5 summarises $\mathcal{A} \times \varepsilon$ for a number
686 of benchmark models, each chosen to be near the limit of search sensitivity. For each topology,
687 typically two different pairs of parent sparticle and LSP masses ($m_{\text{SUSY}}, m_{\text{LSP}}$) are chosen that
688 are characterised by a large and a smaller (i.e. "compressed") difference in parent sparticle and
689 LSP masses. The four most sensitive event categories, defined in terms of n_{jet}, are used to de-
690 termine σ_{UL}. The categories used per benchmark model are listed in Table 5, along with $\mathcal{A} \times \varepsilon$
691 determined for these four categories.

692 Contributions from several sources to the uncertainty in $\mathcal{A} \times \varepsilon$ are considered. Each source of
693 uncertainty is included in the likelihood function via alternative shapes to the nominal $H_{\text{T}}^{\text{miss}}$
694 templates evaluated from simulated signal events categorised according to n_{jet}, n_{b}, and H_{T}.
695 Correlations are taken into account where appropriate, including those relevant to signal con-

Table 5: A summary of benchmark simplified models, the most sensitive n_{jet} categories, and representative values for the corresponding experimental acceptance times efficiency ($\mathcal{A} \times \varepsilon$), the dominant sysmtematic uncertainties, the theory production cross section (σ_{theory}), and the expected and observed upper limits on the production cross section, expressed in terms of the signal strength parameter (μ).

Benchmark models ($m_{\text{SUSY}}, m_{\text{LSP}}$) [GeV]		Most sensitive n_{jet} categories	$\mathcal{A} \times \varepsilon$ [%]	Systematic uncertainties [%]				σ_{theory} [fb]	μ (95% CL)	
				MC stat.	ISR	JEC	SF$_{\text{b-tag}}$		Exp.	Obs.
T1qqqq	(1300, 100)	≥5, 4, 3, 2	9.4	7-30	2-2	4-21	2-14	46.1	0.79	0.76
	(900, 700)	≥5, ≥5a, 4, 4a	5.6	10-33	1-13	1-26	1-10	677	0.58	0.44
T2qq_8fold	(1050, 100)	≥5, 3, 2, 4	13.4	7-33	2-5	3-16	1-11	44.0	0.72	0.50
	(650, 550)	≥5, 4, ≥5a, 4a	2.6	10-28	3-9	2-28	1-6	1080	0.74	0.64
T2qq_1fold	(1050, 100)	≥5, 3, 2, 4	17.9	7-33	2-5	3-16	1-11	44.0	0.72	0.50
	(650, 550)	≥5, 4, ≥5a, 4a	2.6	10-28	3-9	2-28	1-6	1080	0.74	0.64
T1bbbb	(1500, 100)	≥5, 4, 3, 2	10.1	5-17	1-2	1-12	2-22	14.2	0.81	0.79
	(1000, 800)	≥5, 4, ≥5a, 4a	4.9	8-31	1-17	1-40	1-14	325	0.33	0.32
T1tttt	(1300, 100)	≥5, ≥5a, 4, 3	2.4	7-16	1-2	2-7	2-12	46.1	1.00	1.89
	(800, 400)	≥5, ≥5a, 4, 4a	0.6	7-27	1-2	3-45	1-8	1490	0.56	1.03
T1ttbb	(1300, 100)	≥5, 4, 3, ≥5a	3.8	9-32	1-2	3-16	2-19	46.1	0.60	0.91
	(1000, 700)	≥5, ≥5a, 4, 3	3.4	9-30	1-9	3-65	1-14	325	0.51	0.70
T5tttt	(800, 100)	≥5, ≥5a, 3, 4	0.2	12-20	2-4	3-5	1-6	1490	0.69	1.19
	(700, 400)	≥5, ≥5a, 4, 4a	0.2	20-29	2-10	8-10	1-2	3530	1.00	1.35
T5ttcc	(1200, 200)	≥5, 4, 3, ≥5a	4.9	6-25	5-25	3-21	1-24	85.6	0.58	0.87
	(750, 600)	≥5, ≥5a, 4, 4a	1.0	9-23	1-4	5-21	1-3	2270	0.89	0.72
T5tttt_degen	(1100, 100)	≥5, 4, 3, 4a	1.3	15-21	12-16	6-11	4-15	16.3	0.89	2.55
	(800, 600)	≥5, ≥5a, 4a, 4	1.9	5-32	1-8	1-34	1-7	1490	0.66	0.70
T2bb	(800, 50)	2, 3, 4, ≥5	1.5	5-31	2-6	1-21	1-23	28.3	0.96	1.06
	(375, 300)	≥5, 4, 3a, 3	0.1	8-33	1-10	3-25	1-7	2610	0.67	0.87
T2tb	(600, 50)	≥5, 4, 3, 2	6.1	3-28	1-3	1-22	1-17	175	0.70	1.35
	(350, 225)	≥5, 4, 3, 3a	1.0	9-33	1-4	2-41	1-8	3790	0.79	0.88
T2tt	(700, 50)	≥5, 4, 3, ≥5a	8.1	8-33	1-4	2-22	1-21	67.0	0.90	1.19
	(350, 100)	≥5, ≥5a, 4a, 4	1.4	7-31	1-1	1-28	1-7	3790	0.44	0.50
T2cc	(325, 305)	≥5, 4, 3, 2	0.8	3-32	1-27	1-27	1-12	5600	0.92	0.68
T2_degen	(300, 290)	3, 4, ≥5, 2	0.9	2-27	1-27	1-25	1-12	8520	0.56	0.41
T2tt_mixed	(300, 250)	≥5, 4, ≥5a, 4a	0.4	3-33	1-27	1-33	1-13	8520	0.99	0.58

tamination in the control regions. The morphing scheme that interpolates between the nominal and alternative $H_{\text{T}}^{\text{miss}}$ templates, described in Section 7, is also used for the simulated signal samples.

In addition to the uncertainty in the integrated luminosity of 4.6% [?], the following sources of uncertainty are dominant: the statistical uncertainty arising from the finite size of simulated signal samples, the modelling of initial-state radiation (ISR), the corrections to jet energies (JEC) evaluated in simulation, and the modelling of scale factors (SF$_{\text{b-tag}}$) applied to simulated event samples that correct for differences in the efficiency and misidentification probability of b quark jets. The magnitude of each contribution depends on the model and the masses of the parent sparticle and LSP.

The $\mathcal{A} \times \varepsilon$ for models with small mass splittings (e.g. $m_{\widetilde{q}} - m_{\widetilde{\chi}_1^0} \lesssim m_{\text{t}}$) is due in large part

to ISR, the modelling of which is evaluated by comparing the simulated and measured p_T spectra of the system recoiling against the ISR jets in $t\bar{t}$ events, using the technique described in Ref. [59]. The uncertainty can be as large as $\sim$30%, and is the dominant systematic uncertainty for systems with a compressed mass spectrum. Uncertainties in the jet energy scale, as large as $\sim$40%, can also be dominant for models characterised by high jet multiplicities in the final state. The uncertainties in $SF_{b\text{-tag}}$ can be as large as $\sim$25%. Table 5 summarises these dominant contributions to the uncertainty in $\mathcal{A} \times \varepsilon$ for a range of benchmark models. Characteristic values for each model are expressed in terms of a range that is representative of the values across all bins of the signal region. The upper bound for each range may be subject to moderate statistical fluctuations.

Further uncertainties with subdominant contributions are considered on a similar footing. The uncertainties in the efficiency of identifying well-reconstructed, isolated leptons are considered, with a typical magnitude of $\sim$5% and treated as anti-correlated between the signal and control regions. An uncertainty of 5% in the minimum bias cross section, $\sigma_{MB} = 69.0 \pm 3.5$ mb, is assumed and propagated through to the reweighting procedure to account for differences between the simulated and data-derived measurements of the pileup distributions. Finally, uncertainties in the simulation modelling of the efficiencies of the trigger strategy employed by the search are typically <10%.

The choice of PDF set, or variations therein, predominantly affects $\mathcal{A} \times \varepsilon$ through changes in the p_T spectrum of the system recoil, which is covered by the ISR uncertainty, hence no additional uncertainty is adopted. Uncertainties in $\mathcal{A} \times \varepsilon$ due to variations in the renormalisation and factorisation scales are determined to be relatively small. In both cases, contributions to the uncertainty in the theory production cross section are considered.

8.3   Cross section and mass exclusions

The upper limits on the signal production cross section are evaluated at a 95% CL for each of the aforementioned benchmark models. The limits are expressed in terms of the signal strength parameter, μ, which is determined relative to the theory cross section that is calculated at NLO+NLL accuracy. The limits are summarised in Table 5. Expected limits on μ are also listed, which are determined using an asimov data set. All benchmark models are disfavoured based on expectations. The observed limits fluctuate around the expected μ values, with some models exhibiting a moderately weaker-than-expected limit due to fluctuations in data, as discussed below.

Figures 7 and 8 summarise the disfavoured regions of the mass parameter space for fifteen simplified models. These regions are derived by comparing the upper limits on the measured fiducial cross section, corrected for the experimental $\mathcal{A} \times \varepsilon$, with the theory cross sections calculated at NLO+NLL accuracy in α_s. The former cross section value is determined as a function of $m_{\tilde{g}}$ or $m_{\tilde{q}}$ and $m_{\tilde{\chi}_1^0}$, while the latter has a dependence solely on $m_{\tilde{g}}$ or $m_{\tilde{q}}$. For each simplifed model, exclusion contours in the mass plane are shown when evaluated with the observed data counts in the signal region (solid contours) and the expected counts based on an asimov data set (dashed contours).

Figure 7 (top) shows exclusion contours for models that assume the gluino-mediated or direct production of light-flavour squarks. The excluded region extends to higher masses for the gluino-mediated production of light-flavour squarks (T1qqqq), with respect to the direct pair production when assuming an eightfold degeneracy in mass (T2qq_8fold), due to a combination of a higher gluino pair production cross section and a final state characterised by higher jet multiplicities, which can be exploited to provide better signal-to-background seperation.
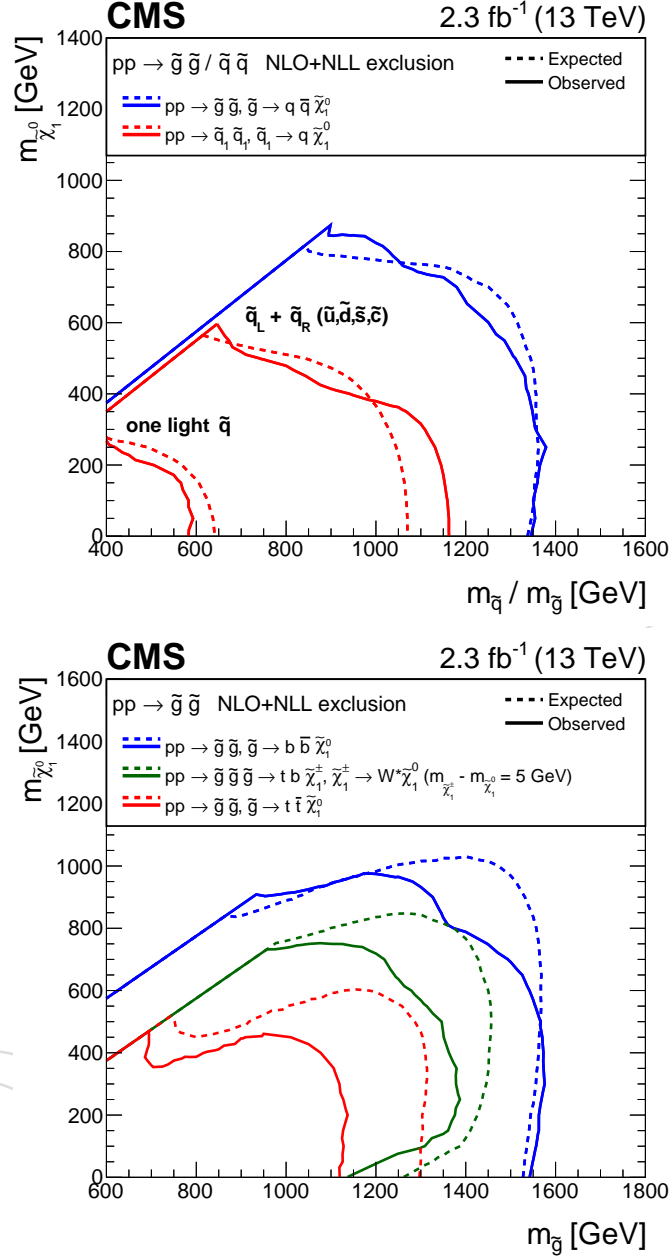
Figure 7: Observed and expected mass exclusions at 95% CL (indicated, respectively, by solid and dashed contours) for a number of simplified models. (Top) The pair production of gluino-mediated or direct pair production of light-flavour squarks. The two scenarios involve, respectively, the decay $\widetilde{g} \to \bar{q}q\widetilde{\chi}_1^0$ (T1qqqq) and $\widetilde{q} \to q\widetilde{\chi}_1^0$, and the latter involves two assumptions on the mass degeneracy of the squarks (T2qq_8fold and T2qq_1fold). (Bottom) Three scenarios involving the gluino-mediated pair production of off-shell third-generation squarks: $\widetilde{g} \to \bar{b}b\widetilde{\chi}_1^0$ (T1bbbb), $\widetilde{g} \to \widetilde{t}\bar{t}^* \to \bar{t}t\widetilde{\chi}_1^0$ (T1tttt), and $\widetilde{g} \to \bar{t}b\widetilde{\chi}_1^\pm \to \bar{t}bW^*\widetilde{\chi}_1^0$ (T1tbb).

The excluded mass region is significantly reduced when assuming only a single light squark (T2qq_1fold), with limits weakening due to the lower production cross section, compounded by the reduced signal-to-background ratios achieved in the core of distributions in the discrim-
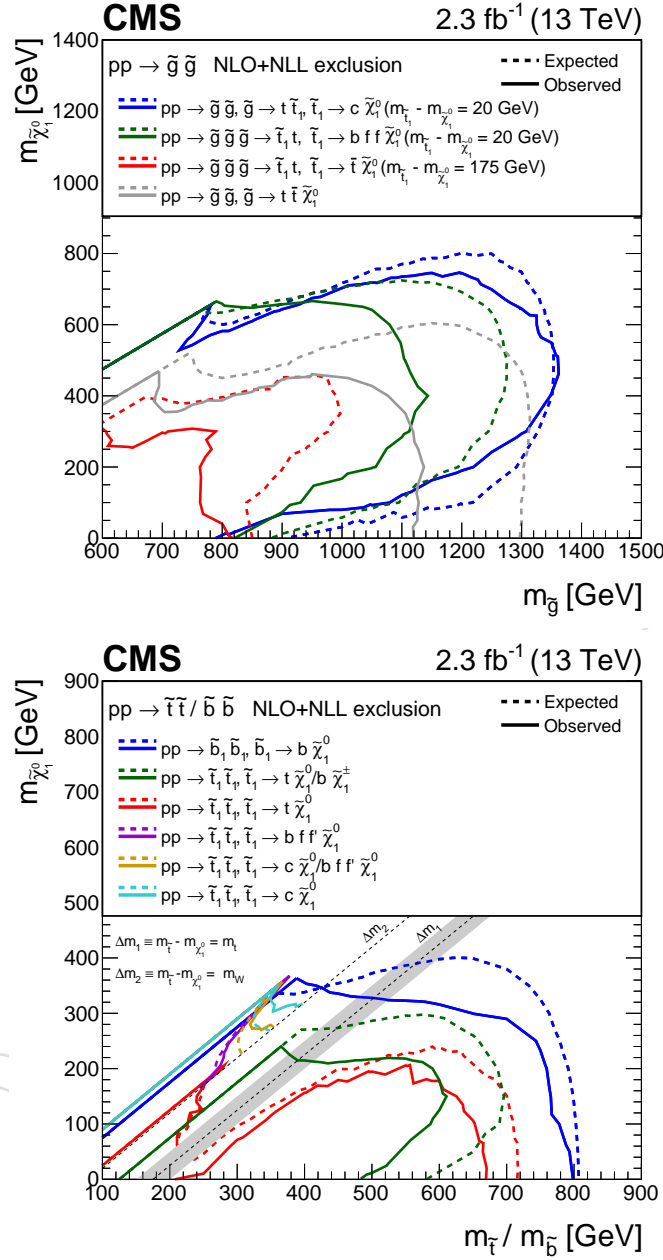
Figure 8: Observed and expected mass exclusions at 95% CL (indicated, respectively, by solid and dashed contours) for a number of simplified models. (Top) Three scenarios involving the gluino-mediated pair production of on-shell top squarks: $\widetilde{g} \rightarrow \overline{t}\widetilde{t} \rightarrow \overline{t}t\widetilde{\chi}_1^0$ with $m_{\widetilde{t}} - m_{\widetilde{\chi}_1^0} = 175\,\text{GeV}$ (T5tttt), $\widetilde{g} \rightarrow \overline{t}\widetilde{t} \rightarrow \overline{t}c\widetilde{\chi}_1^0$ with $m_{\widetilde{t}} - m_{\widetilde{\chi}_1^0} = 20\,\text{GeV}$ (T5ttcc), and $\widetilde{g} \rightarrow \overline{t}\widetilde{t} \rightarrow \overline{t}bW^*\widetilde{\chi}_1^0$ with $m_{\widetilde{t}} - m_{\widetilde{\chi}_1^0} = 20\,\text{GeV}$ (T5tttt_degen). (Bottom) Six scenarios involving the direct pair production of third-generation squarks. The first scenario involves the pair production of bottom squarks, $\widetilde{b} \rightarrow b\widetilde{\chi}_1^0$ (T2bb). Two scenarios involve the decay of top squark pairs as follows: $\widetilde{t} \rightarrow t\widetilde{\chi}_1^0$ or $\widetilde{t} \rightarrow b\widetilde{\chi}_1^\pm \rightarrow bW^*\widetilde{\chi}_1^0$ with $m_{\widetilde{\chi}_1^\pm} - m_{\widetilde{\chi}_1^0} = 5\,\text{GeV}$ and $\mathcal{BR} = 50/50\%$ (T2tb), or $\widetilde{t} \rightarrow t\widetilde{\chi}_1^0$ (T2tt). The final three sceanarios consider top squark decays under the assumption $10 < m_{\widetilde{t}} - m_{\widetilde{\chi}_1^0} < 80\,\text{GeV}$: $\widetilde{t} \rightarrow c\widetilde{\chi}_1^0$ (T2cc), $\widetilde{t} \rightarrow bW^*\widetilde{\chi}_1^0$ (T2tt_degen), and $\widetilde{t} \rightarrow c\widetilde{\chi}_1^0$ or $\widetilde{t} \rightarrow bW^*\widetilde{\chi}_1^0$ with $\mathcal{BR} = 50/50\%$ (T2tt_mixed).

756   inating variables.

757   Figure 7 (bottom) shows exclusion contours for models that assume the gluino-mediated pair
758   production of off-shell third-generation squarks. For the topologies T1tttt and T1bbbb, each
759   gluino is assumed to undergo a three-body decay via, respectively, an off-shell top or bottom
760   squark to a quark-antiquark pair of the same flavour and the $\widetilde{\chi}_1^0$. In the case of T1ttbb, each
761   gluino is assumed to undergo a three-body decay to an on-shell chargino, $\widetilde{\chi}_1^\pm$, a bottom quark,
762   and an antitop quark. The chargino mass is defined relative to the neutralino mass via the
763   expression $m_{\widetilde{\chi}_1^\pm} - m_{\widetilde{\chi}_1^0} = 5\,\text{GeV}$. The chargino decays promptly to the $\widetilde{\chi}_1^0$ and an off-shell W
764   boson. The excluded mass regions differ significantly for these topologies, primarily due to the
765   different number of (on-shell) W bosons in their final states, resulting in the highest $\mathcal{A} \times \varepsilon$ for
766   T1bbbb and lowest for T1tttt. Further, $\mathcal{A} \times \varepsilon$ has a strong dependence on jet multiplicity,
767   which is highest for T1tttt, due to the $\Delta\phi_{\min}^*$ variable. An additional feature for T1ttbb is
768   the weakening of the mass limit at low values of $m_{\widetilde{\chi}_1^0}$, when $m_{\widetilde{\chi}_1^\pm} = m_{\widetilde{\chi}_1^0} + 5\,\text{GeV} \lesssim m_\text{t}$. In this
769   scenario, the $\widetilde{\chi}_1^\pm$ (and hence $\widetilde{\chi}_1^0$) is not highly Lorentz boosted relative to the top quark resulting
770   from the three-body decay of the gluino. Hence, two $\widetilde{\chi}_1^0$ sparticles do not carry away significant
771    $\vec{p}_\text{T}^{\text{miss}}$, which is instead realised through W boson decays to neutrinos and "lost" leptons or τ
772   leptons that decay to neutrinos and hadrons. The observed mass limits for these topologies
773   are up to $\sim$2 standard deviations weaker than the expected limits. These differences are due
774   to upward fluctuations in data for two contiguous bins that satisfy the requirements $n_\text{jet} \geq 5$,
775    $n_\text{b} \geq 2$, and $H_\text{T} > 800\,\text{GeV}$. This region has the highest sensitivity to models involving gluino
776   production and decays to third-generation quarks (via on- or off-shell squarks). The observed
777   counts are consistent with statistical fluctuations and the events do not exhibit anomolous non-
778   physical behaviours. The events are distributed in H_T^{miss} consistent with expectation, hence
779   models characterised by high values of H_T^{miss}, such as T1bbbb with $m_{\widetilde{\text{g}}} \gg m_{\widetilde{\chi}_1^0}$ or $m_{\widetilde{\text{g}}} \approx m_{\widetilde{\chi}_1^0}$,
780   are less compatible with the data counts in this high-n_jet, n_b, and H_T region.

781   Figure 8 (top) shows exclusion contours for models that assume gluino pair production, with
782   each gluino decaying to a top quark and an on-shell top squark, the latter of which decays to
783   SM particles and the LSP, $\widetilde{\chi}_1^0$. As discussed earlier, these models can be considered as repre-
784   sentations of a "natural" solution to the little hierarchy problem. Three different scenarios are
785   considered for the decay of the top squarks. The T5tttt model assumes a two-body decay to a
786   top quark and the $\widetilde{\chi}_1^0$, with the top squark mass defined relative to the $\widetilde{\chi}_1^0$ as $m_{\widetilde{\text{t}}} - m_{\widetilde{\chi}_1^0} = m_\text{t}$. The
787   T5ttcc and T5tttt_degen models assume $m_{\widetilde{\text{t}}} - m_{\widetilde{\chi}_1^0} = 20\,\text{GeV}$ and two- and four-body de-
788   cays to, respectively, a charm quark and the $\widetilde{\chi}_1^0$, or to $\text{bff}'\widetilde{\chi}_1^0$ via an off-shell W boson. These two
789   decays are the only modes open to the top squark under this near-mass-degenerate scenario.

790   Finally, Fig. 8 (bottom) shows exclusion contours for models that assume the direct production
791   of pairs of third-generation squarks. For the model T2bb, bottom squarks are pair produced
792   and each decays to a bottom quark and the $\widetilde{\chi}_1^0$. The model T2tt assumes top squarks are pair
793   produced and each is assumed to undergo a two- or three-body decay to, respectively, a top
794   quark and the $\widetilde{\chi}_1^0$ when $m_{\widetilde{\text{t}}} - m_{\widetilde{\chi}_1^0} > m_\text{t}$ is satisfied, or a b quark, an on-shell W boson, and
795   the $\widetilde{\chi}_1^0$ for the condition $m_\text{W} < m_{\widetilde{\text{t}}} - m_{\widetilde{\chi}_1^0} < m_\text{t}$. Models that satisfy $|m_{\widetilde{\text{t}}} - m_\text{t} - m_{\widetilde{\chi}_1^0}| < 25\,\text{GeV}$
796   are not considered here. The model T2tb also assumes the pair production of top squarks,
797   with each undergoing a two-body decay to either a top quark and the $\widetilde{\chi}_1^0$, or a bottom quark
798   and the $\widetilde{\chi}_1^\pm$, with equal branching ratios $\mathcal{BR}(\widetilde{\text{t}} \to \text{t}\widetilde{\chi}_1^0) = \mathcal{BR}(\widetilde{\text{t}} \to \text{b}\widetilde{\chi}_1^\pm) = 50\%$. As for the
799   T1ttbb model, the chargino mass is defined relative to the neutralino mass via the expression
800    $m_{\widetilde{\chi}_1^\pm} - m_{\widetilde{\chi}_1^0} = 5\,\text{GeV}$, and the chargino decays promptly to the $\widetilde{\chi}_1^0$ and an off-shell W boson.
801   The excluded mass regions differ significantly for the T2bb, T2tb, and T2tt topologies, in an
802   analogous way to the T1bbbb, T1ttbb, and T1tttt models described above. The difference

in the mass exclusions is due primarily to the different number of (on-shell) W bosons in the final states, which affects $\mathcal{A} \times \varepsilon$ through the presence of leptons from the decay of the W boson. Further, an additional feature for T2tb is the weakening of the mass limit at low values of $m_{\widetilde{\chi}_1^0}$, when $m_{\widetilde{\chi}_1^\pm} = m_{\widetilde{\chi}_1^0} + 5 \, \text{GeV} \lesssim m_\text{t}$. Moderately weaker-than-expected mass limits are observed for all models involving two-body decays, which is traced to mild upward fluctuations in data for events satisfying $n_\text{jet} = 2$, $n_\text{b} = 2$, and $350 < H_\text{T} < 500 \, \text{GeV}$.

Figure 8 (bottom) also shows exclusion contours for models that assume the pair production of top squarks but a near-mass-degenerate system that satisfies $10 \, \text{GeV} < m_{\widetilde{\text{t}}} - m_{\widetilde{\chi}_1^0} < m_\text{W}$. Two decays of the top squark are considered. Analogous to the T5ttcc and T5tttt_degen models (but without the gluino), the T2cc and T2tt_degen models assume two- and four-body decays of the top squark to, respectively, a charm quark and the $\widetilde{\chi}_1^0$, or to via an off-shell W boson. A third model, T2tt_mixed, assumes both these decay modes with an equal branching ratio, $\mathcal{BR}(\widetilde{\text{t}} \to \text{c}\widetilde{\chi}_1^0) = \mathcal{BR}(\widetilde{\text{t}} \to \text{bff}'\widetilde{\chi}_1^0) = 50\%$. For T2cc, the excluded mass region is relatively stable as a function of the mass splitting $\Delta m = m_{\widetilde{\text{t}}} - m_{\widetilde{\chi}_1^0}$, with $\widetilde{\text{t}}$ masses excluded up to $400 \, \text{GeV}$. For T2tt_degen, the excluded mass region is strongly dependent on Δm, weakening considerably for increasing values of Δm due to the increased momentum phase space available to leptons produced in the four-body decay. The model T2tt_mixed exhibits an intermediate behaviour. Mass limits for all three models converge for the smallest mass splitting considered, $\Delta m = 10 \, \text{GeV}$, when the SM particles from the $\widetilde{\text{t}}$ decay are extremely soft and outside the experimental acceptance. An approximately contiguous mass exclusion limit is observed across the transition from the T2tt_degen four-body to the T2tt three-body decay of the $\widetilde{\text{t}}$, as the top quark moves on-shell. The excluded mass region weakens further as $\Delta m \to m_\text{t}$.

Table 6 summarises the strongest expected and observed excluded $m_{\widetilde{\text{g}}}$ or $m_{\widetilde{\text{q}}}$ and $m_{\widetilde{\chi}_1^0}$ masses for each simplified model.

9 Summary

An inclusive search for new-physics phenomena is reported, based on data from pp collisions at $\sqrt{s} = 13 \, \text{TeV}$. The data are recorded with the CMS detector and correspond to an integrated luminosity of $2.3 \pm 0.1 \, \text{fb}^{-1}$. The final states analysed contain one or more jets with large transverse momenta (p_T) and a significant imbalance in transverse momentum, as expected from the production of massive coloured sparticles, each decaying to SM particles and the lightest supersymmetric particle.

Signal candidate events are categorised according to the number of reconstructed jets, and the number of jets identified as originating from b quarks, and the scalar (H_T) and vector (H_T^miss) sums of the transverse momenta of jets. The search employs the use of several kinematic variables, including α_T and $\Delta\phi_\text{min}^*$, to suppress the background from QCD multijet production to the percent level with respect to other nonmultijet SM backgrounds, which are dominated by vector boson and top-antitop production. The α_T variable is also employed in the trigger logic that is used to record the candidate signal events, which allows the use of low thresholds for the momentum sums, $H_\text{T} > 200 \, \text{GeV}$ and $H_\text{T}^\text{miss} \gtrsim 130 \, \text{GeV}$. These low thresholds, in addition to the inclusive of final states containing a single jet, maximise the experimental acceptance to new-physics processes, such as low-mass squark signatures, nearly mass-degenerate SUSY models, and other new-physics phenomena, such as DM models that postulate the direct production of stable, weakly interacting, massive particles in pp collisions.

Table 6: Summary of the mass limits obtained for the fifteen simplified models. The limits indicate the strongest observed and expected (in parentheses) mass exclusions in $\widetilde{g}$, $\widetilde{q}$, $\widetilde{b}$, $\widetilde{t}$, and $\widetilde{\chi}_1^0$. The quoted values have uncertainties of $\pm 25\,\mathrm{GeV}$ and $\pm 10\,\mathrm{GeV}$ for models involving the pair production of, respectively, gluinos and squarks.

Topology	Parent sparticle	Best mass limit [GeV] $\widetilde{g}/\widetilde{q}/\widetilde{b}/\widetilde{t}$	$\widetilde{\chi}_1^0$
T1qqqq	$\widetilde{g}$	1375 (1350)	875 (850)
T2qq_8fold	$\widetilde{q}$	1150 (1075)	600 (550)
T2qq_1fold	$\widetilde{q}$	575 (650)	275 (275)
T1bbbb	$\widetilde{g}$	1575 (1575)	975 (1025)
T1tttt	$\widetilde{g}$	1125 (1325)	475 (600)
T1ttbb	$\widetilde{g}$	1375 (1450)	750 (850)
T5tttt	$\widetilde{g}$	800 (1000)	300 (450)
T5ttcc	$\widetilde{g}$	1350 (1350)	700 (800)
T5tttt_degen	$\widetilde{g}$	1150 (1275)	650 (725)
T2bb	$\widetilde{b}$	800 (800)	360 (400)
T2tb	$\widetilde{t}$	610 (690)	240 (300)
T2tt (3-body)	$\widetilde{t}$	670 (720)	210 (240)
T2tt (2-body)	$\widetilde{t}$	280 (280)	200 (200)
T2cc	$\widetilde{t}$	400 (350)	310 (340)
T2tt_degen	$\widetilde{t}$	370 (360)	360 (350)
T2tt_mixed	$\widetilde{t}$	360 (350)	350 (340)

The sums of the standard model backgrounds are estimated from a simultaneous binned likelihood fit to the observed yields for samples of events categorised according to n_{jet}, n_{b}, H_{T}, and $H_{\mathrm{T}}^{\mathrm{miss}}$ in the signal region and in μ+jets, $\mu\mu$+jets, and γ+jets control regions. The observed yields in the signal are found to be in agreement with the expected contributions from standard model processes. The search result is interpreted in the mass parameter space of fifteen simplified supersymmetric models that assume the pair production of gluinos or squarks and a range of decay modes. The models cover scenarios that involve the gluino-mediated or direct production or light- or heavy-flavour squarks, spectra with intermediate sparticle states and branching ratios, "natural" spectra with gluinos and on-shell top squarks, and nearly mass-degenerate spectra.

The increase in the centre-of-mass energy of the LHC, from $\sqrt{s} = 8$ to $13\,\mathrm{TeV}$, provides a significant gain in sensitivity to heavy particle states such as gluinos. In the case of pair production of gluinos that each decays, via an off-shell b squark, to the b quark and the LSP, masses up to $\sim 1.6\,\mathrm{TeV}$ and $\sim 1.0\,\mathrm{TeV}$ are excluded for, respectively, the gluino and LSP. In the case of direct pair production, masses up to $\sim 800\,\mathrm{GeV}$ and $\sim 350\,\mathrm{GeV}$ are excluded for, respectively, the b squark and LSP. These mass limits are sensitive to the assumptions on the squark flavour and the presence of intermediate states, such as charginos.

Finally, a comprehensive study of nearly mass-degenerate models involving top squark pair production is performed. The two decay modes open to the top squark are considered: the loop-induced two-body decay to the neutralino and one c quark, and the four-body decay to the neutralino, one b quark, and an off-shell W boson. A third scenario is considered, when the two modes are simultaneously open each with a branching ratio of 50%. Masses of the top squark and LSP up to, respectively, $400\,\mathrm{GeV}$ and $360\,\mathrm{GeV}$ are excluded, depending on the decay modes considered.

In summary, the analysis provides sensitivity across a large region of the "natural" supersym-

metric parameter space, as characterised by interpretations with several simplified models. In particular, these studies improve on existing limits for nearly mass-degenerate models involving the production of pairs of top squarks.

References

[1] Y. A. Gol'fand and E. P. Likhtman, "Extension of the Algebra of Poincaré Group Generators and Violation of p Invariance", *JETP Lett.* **13** (1971) 323.

[2] J. Wess and B. Zumino, "Supergauge transformations in four dimensions", *Nucl. Phys. B* **70** (1974) 39, doi:10.1016/0550-3213(74)90355-1.

[3] H. P. Nilles, "Supersymmetry, Supergravity and Particle Physics", *Phys. Reports* **110** (1984) 1, doi:10.1016/0370-1573(84)90008-5.

[4] H. Haber and G. Kane, "The Search for Supersymmetry: Probing Physics Beyond the Standard Model", *Phys. Reports* **117** (1987) 75, doi:10.1016/0370-1573(85)90051-1.

[5] R. Barbieri, S. Ferrara, and C. A. Savoy, "Gauge Models with Spontaneously Broken Local Supersymmetry", *Phys. Lett. B* **119** (1982) 343, doi:10.1016/0370-2693(82)90685-2.

[6] S. Dawson, E. Eichten, and C. Quigg, "Search for Supersymmetric Particles in Hadron - Hadron Collisions", *Phys. Rev. D* **31** (1985) 1581, doi:10.1103/PhysRevD.31.1581.

[7] E. Witten, "Dynamical Breaking of Supersymmetry", *Nucl. Phys. B* **188** (1981) 513, doi:10.1016/0550-3213(81)90006-7.

[8] S. Dimopoulos and H. Georgi, "Softly Broken Supersymmetry and SU(5)", *Nucl. Phys. B* **193** (1981) 150, doi:10.1016/0550-3213(81)90522-8.

[9] ATLAS Collaboration, "Observation of a new particle in the search for the Standard Model Higgs boson with the ATLAS detector at the LHC", *Phys. Lett. B* **716** (2012) 1, doi:10.1016/j.physletb.2012.08.020, arXiv:1207.7214.

[10] CMS Collaboration, "Observation of a new boson with mass near 125 GeV in pp collisions at $\sqrt{s} = 7$ and 8 TeV", *JHEP* **06** (2013) 081, doi:10.1007/JHEP06(2013)081, arXiv:1303.4571.

[11] G. R. Farrar and P. Fayet, "Phenomenology of the Production, Decay, and Detection of New Hadronic States Associated with Supersymmetry", *Phys. Lett. B* **76** (1978) 575, doi:10.1016/0370-2693(78)90858-4.

[12] CMS Collaboration, "Search for Supersymmetry in pp Collisions at 7 TeV in Events with Jets and Missing Transverse Energy", *Phys. Lett. B* **698** (2011) 196, doi:10.1016/j.physletb.2011.03.021, arXiv:1101.1628.

[13] CMS Collaboration, "Search for Supersymmetry at the LHC in Events with Jets and Missing Transverse Energy", *Phys. Rev. Lett.* **107** (2011) 221804, doi:10.1103/PhysRevLett.107.221804.

[14] CMS Collaboration, "Search for supersymmetery in final states with missing transverse energy and 0, 1, 2, or ≥ 3 b-quark jets in 7 TeV pp collisions using the α_T variable", *JHEP* **01** (2013) 077, `doi:10.1007/JHEP01(2013)077`.

[15] CMS Collaboration, "Search for supersymmetry in hadronic final states with missing transverse energy using the variables α_T and b-quark multiplicity in pp collisions at $\sqrt{s} = 8$ TeV", *EPJC* **01** (2013) 077, `doi:10.1007/JHEP01(2013)077`.

[16] P. J. Fox, R. Harnik, R. Primulando, and C.-T. Yu, "Taking a Razor to Dark Matter Parameter Space at the LHC", *Phys. Rev.* **D86** (2012) 015010, `doi:10.1103/PhysRevD.86.015010`, `arXiv:1203.1662`.

[17] O. Buchmueller, S. A. Malik, C. McCabe, and B. Penning, "Constraining Dark Matter Interactions with Pseudoscalar and Scalar Mediators Using Collider Searches for Multijets plus Missing Transverse Energy", *Phys. Rev. Lett.* **115** (2015), no. 18, 181802, `doi:10.1103/PhysRevLett.115.181802`, `arXiv:1505.07826`.

[18] L. Randall and D. Tucker-Smith, "Dijet Searches for Supersymmetry at the Large Hadron Collider", *Phys. Rev. Lett.* **101** (2008) 221803, `doi:10.1103/PhysRevLett.101.221803`, `arXiv:0806.1049`.

[19] CMS Collaboration, "The CMS experiment at the CERN LHC", *JINST* **3** (2008) S08004, `doi:10.1088/1748-0221/3/08/S08004`.

[20] J. Alwall et al., "The automated computation of tree-level and next-to-leading order differential cross sections, and their matching to parton shower simulations", *Journal of High Energy Physics* **07** (2014) 079, `doi:10.1007/JHEP07(2014)079`, `arXiv:1405.0301`.

[21] S. Alioli, P. Nason, C. Oleari, and E. Re, "A general framework for implementing NLO calculations in shower Monte Carlo programs: the POWHEG BOX", *JHEP* **06** (2010) 043, `doi:10.1007/JHEP06(2010)043`, `arXiv:1002.2581`.

[22] E. Re, "Single-top Wt-channel production matched with parton showers using the POWHEG method", *Eur. Phys. J. C* **71** (2011) 1547, `doi:10.1140/epjc/s10052-011-1547-z`, `arXiv:1009.2450`.

[23] R. Gavin, Y. Li, F. Petriello, and S. Quackenbush, "W Physics at the LHC with FEWZ 2.1", *Comput. Phys. Commun.* **184** (2013) 208, `doi:10.1016/j.cpc.2012.09.005`, `arXiv:1201.5896`.

[24] R. Gavin, Y. Li, F. Petriello, and S. Quackenbush, "FEWZ 2.0: A code for hadronic Z production at next-to-next-to-leading order", *Comput. Phys. Commun.* **182** (2011) 2388, `doi:10.1016/j.cpc.2011.06.008`, `arXiv:1011.3540`.

[25] T. Melia, P. Nason, R. Rontsch, and G. Zanderighi, "W^+W^-, WZ and ZZ production in the POWHEG BOX", *JHEP* **11** (2011) 078, `doi:10.1007/JHEP11(2011)078`, `arXiv:1107.5051`.

[26] C. M. and A. Mitov, "Top++: A program for the calculation of the top-pair cross-section at hadron colliders", *Comput. Phys. Commun.* **185** (2014) 2930, `doi:10.1016/j.cpc.2014.06.021`, `arXiv:1112.5675`.

[27] S. Alioli, P. Nason, C. Oleari, and E. Re, "NLO single-top production matched with shower in POWHEG: s- and t-channel contributions", *JHEP* **09** (2009) 111, doi:10.1088/1126-6708/2009/09/111, arXiv:0907.4076.

[28] S. Agostinelli et al., "GEANT4 — a simulation toolkit", *Nucl. Instr. and Meth. A* **506** (2003) 250, doi:10.1016/S0168-9002(03)01368-8.

[29] T. Sjöstrand et al., "An Introduction to PYTHIA 8.2", *Comput. Phys. Commun.* **191** (2015) 159, doi:10.1016/j.cpc.2015.01.024, arXiv:1410.3012.

[30] W. Beenakker, R. Höpker, M. Spira, and P. M. Zerwas, "Squark and gluino production at hadron colliders", *Nucl. Phys. B* **492** (1997) 51, doi:10.1016/S0550-3213(97)00084-9.

[31] A. Kulesza and L. Motyka, "Threshold Resummation for Squark-Antisquark and Gluino-Pair Production at the LHC", *Phys. Rev. Lett.* **102** (2009) 111802, doi:10.1103/PhysRevLett.102.111802.

[32] A. Kulesza and L. Motyka, "Soft gluon resummation for the production of gluino-gluino and squark-antisquark pairs at the LHC", *Phys. Rev. D* **80** (2009) 095004, doi:10.1103/PhysRevD.80.095004.

[33] W. Beenakker et al., "Soft-gluon resummation for squark and gluino hadroproduction", *JHEP* **09** (2009) 041, doi:10.1088/1126-6708/2009/12/041.

[34] W. Beenakker et al., "Squark and gluino hadroproduction", *Int. J. Mod. Phys. A* **26** (2011) 2637, doi:10.1142/S0217751X11053560.

[35] C. Borschensky et al., "Squark and gluino production cross sections in pp collisions at $\sqrt{s} = 13, 14, 33$ and 100 TeV", *Eur. Phys. J. C* **74** (2014) 3174, doi:10.1140/epjc/s10052-014-3174-y, arXiv:1407.5066.

[36] CMS Collaboration, "The fast simulation of the CMS detector at LHC", *J. Phys. Conf. Ser.* **331** (2011) 032049, doi:10.1088/1742-6596/331/3/032049.

[37] NNPDF Collaboration, "Parton distributions for the LHC Run II", *JHEP* **04** (2015) 040, doi:10.1007/JHEP04(2015)040, arXiv:1410.8849.

[38] CMS Collaboration, "Particle-flow event reconstruction in CMS and performance for jets, taus, and $\not{E}_T$", CMS Physics Analysis Summary CMS-PAS-PFT-09-001, 2009.

[39] CMS Collaboration, "Commissioning of the particle-flow event with the first LHC collisions recorded in the CMS detector", CMS Physics Analysis Summary CMS-PAS-PFT-10-001, 2010.

[40] CMS Collaboration, "Performance of photon reconstruction and identification with the CMS detector in proton-proton collisions at $\sqrt{s} = 8$ TeV", *JINST* **10** (2015) P08010, doi:10.1088/1748-0221/10/08/P08010, arXiv:1502.02702.

[41] CMS Collaboration, "Performance of electron reconstruction and selection with the CMS detector in proton-proton collisions at $\sqrt{s} = 8$ TeV", *JINST* **10** (2015) P06005, doi:10.1088/1748-0221/10/06/P06005, arXiv:1502.02701.

[42] CMS Collaboration, "Performance of CMS muon reconstruction in pp collision events at $\sqrt{s} = 7$ TeV", *JINST* **7** (2012) P10002, doi:10.1088/1748-0221/7/10/P10002, arXiv:1206.4071.

[43] M. Cacciari, G. P. Salam, and G. Soyez, "The anti-k_t jet clustering algorithm", *JHEP* **04** (2008) 063, doi:10.1088/1126-6708/2008/04/063, arXiv:0802.1189.

[44] M. Cacciari and G. P. Salam, "Pileup subtraction using jet areas", *Phys. Lett. B* **659** (2008) 119, doi:10.1016/j.physletb.2007.09.077, arXiv:0707.1378.

[45] CMS Collaboration, "Determination of jet energy calibration and transverse momentum resolution in CMS", *JINST* **6** (2011) P11002, doi:10.1088/1748-0221/6/11/P11002, arXiv:1107.4277.

[46] CMS Collaboration, "Identification of b-quark jets with the CMS experiment", *JINST* **8** (2013) P04013, doi:10.1088/1748-0221/8/04/P04013, arXiv:1211.4462.

[47] CMS Collaboration, "Performance of b-tagging algorithms in 25 ns data at 13 TeV", CMS Detector Performance Summary CMS-DP-2015-056, 2015.

[48] CMS Collaboration, "Missing transverse energy performance of the CMS detector", *JINST* **6** (2011) P09001, doi:10.1088/1748-0221/6/09/P09001, arXiv:1106.5048.

[49] CMS Collaboration, "Identification and filtering of uncharacteristic noise in the CMS hadron calorimeter", *JINST* **5** (2010) T03014, doi:10.1088/1748-0221/5/03/T03014, arXiv:0911.4881.

[50] CMS Collaboration, "Electromagnetic calorimeter commissioning and first results with 7 TeV data", CMS Note CMS-NOTE-2010-012, 2010.

[51] Z. Bern et al., "Driving Missing Data at Next-to-Leading Order", (2011). arXiv:1106.1423.

[52] CERN, "PHYSTAT Workshop on Statistical Issues Related to Discovery Claims in Search Experiments and Unfolding". CERN, Geneva, (2011). doi:10.5170/CERN-2011-006.

[53] J. Alwall, P. Schuster, and N. Toro, "Simplified Models for a First Characterization of New Physics at the LHC", *Phys. Rev. D* **79** (2009) 075020, doi:10.1103/PhysRevD.79.075020.

[54] J. Alwall, M.-P. Le, M. Lisanti, and J. G. Wacker, "Model-independent jets plus missing energy searches", *Phys. Rev. D* **79** (2009) 015005, doi:10.1103/PhysRevD.79.015005.

[55] D. Alves et al., "Simplified models for LHC new physics searches", *J. Phys. G* **39** (2012) 105005, doi:10.1088/0954-3899/39/10/105005.

[56] T. Junk, "Confidence level computation for combining searches with small statistics", *Nucl. Instr. and Meth. A* **434** (1999) 435, doi:10.1016/S0168-9002(99)00498-2.

[57] A. L. Read, "Presentation of search results: the CL_s technique", *J. Phys. G* **28** (2002) 2693, doi:10.1088/0954-3899/28/10/313.

[58] G. Cowan, K. Cranmer, E. Gross, and O. Vitells, "Asymptotic formulae for likelihood-based tests of new physics", *Eur. Phys. J. C* **71** (2011) 1554, doi:10.1140/epjc/s10052-011-1554-0.

[59] S. Chatrchyan et al., "Search for top-squark pair production in the single-lepton final state in pp collisions at $\sqrt{s} = 8$ TeV", *Eur. Phys. J. C* **73** (2013) 2677, doi:10.1140/epjc/s10052-013-2677-2.